



WPI

Creation of a Fish-Friendly Aquatic Hydropower Device Using an Oscillating Hydrofoil

A Major Qualifying Project
submitted to the Faculty of
WORCESTER POLYTECHNIC INSTITUTE
in partial fulfilment of the requirements for the
degree of Bachelor of Science

By

Patrick Chernjavsky
Patricia (Tricia) Smith
Garrett Hughes
Victoria Niedzwiecki

Date: April 6, 2021

Report Submitted to:

Professor Brian J. Sivilonis
Worcester Polytechnic Institute

Worcester Polytechnic Institute This report represents work of WPI undergraduate students submitted to the faculty as evidence of a degree requirement. WPI routinely publishes these reports on its web site without editorial or peer review. For more information about the projects program at WPI, see <http://www.wpi.edu/Academics/Projects>

Abstract

The harnessing of hydropower for use as a clean, marine life compatible energy has been a struggle with conventional hydropower devices. The goal of our project was to design, develop, and test an alternative system to conventional hydro dams and turbines that could effectively harness the power of running water while minimizing adverse effect on aquatic life. This project was completed by using a novel method for hydropower – harnessing the energy of water with an oscillating hydrofoil. By designing, fabricating, and testing this system, our team was able to demonstrate the system’s concept as a fish-friendly, alternative power generation device. Further testing will be needed to create a fully operational system.

Authorship

Section Title	Main Author(s)	Main Editor(s)	Secondary Author(s)	Secondary Editor(s)
Abstract	Patrick	Patrick	NA	Tricia
Introduction	Patrick, Tricia, Garrett, Victoria	Patrick, Tricia, Garrett, Victoria	NA	NA
2.0 & 2.1	Tricia, Patrick	Tricia	Garrett, Victoria	Garrett, Victoria
2.1.1 Geothermal	Tricia	Tricia	NA	Patrick, Garrett, Victoria
2.1.2 Solar	Patrick	Tricia	NA	Garrett, Victoria
2.1.3 Wind	Victoria	Tricia	NA	Patrick, Garrett
2.1.4 Water	Garrett	Tricia	NA	Patrick
2.2 Renewable Energy Applications	Tricia, Patrick	Tricia, Patrick	NA	Garrett, Victoria
2.3 Energy Generation with Oscillations	Tricia, Patrick	Tricia, Patrick	NA	Garrett, Victoria
2.3.1 VIVACE	Patrick, Victoria	Tricia	NA	Garrett
2.3.3 Flapping	Tricia Smith	Tricia		
2.4.1 Piezoelectrics	Tricia	Tricia	NA	Patrick, Garrett, Victoria
2.4.2 Generators	Garrett	Tricia	NA	Patrick
2.5 Energy Storage	Patrick	Patrick	NA	Tricia, Garrett, Victoria
2.6 Adaptability and Optimization	Tricia	Tricia	NA	Garrett, Patrick, Victoria
2.6.1 Hydrofoil Geometry	Tricia	Tricia, Patrick	NA	Garrett
2.6.2 Power Optimization	Patrick	Patrick	NA	Tricia
2.6.3 Fluid Velocity	Garrett	Garrett, Tricia	NA	Patrick
2.6.4 Flapping Actuation	Patrick	Tricia	NA	Garrett
2.7 Background Summary	Patrick	Tricia	Tricia	Garrett
3.1 Design Intent	Tricia	Tricia	Patrick	Garrett
3.2 Design Specifications	Patrick, Tricia	Patrick, Tricia	Garrett	Garrett, Victoria
3.2.1 Power Efficiency	Tricia	Tricia	NA	Garrett
3.2.2 Power Generation	Victoria	Victoria, Tricia	NA	NA

3.2.3 Frame	Patrick, Garrett	Garrett, Tricia	NA	Patrick
3.2.4 Hydrofoil	Patrick	Patrick, Tricia	NA	Garrett
3.2.5 Hydrofoil Actuation	Patrick	Patrick, Tricia	NA	NA
4.1 Power Calculations	Tricia, Garrett	Tricia, Garrett, Patrick	Patrick	NA
4.2 Slider-Crank Mechanism	Victoria	Victoria	NA	Tricia
5.0 Construction	Patrick, Tricia	Patrick, Tricia	Garrett, Victoria	Garrett, Victoria
6.1 Measurement Systems	Garrett, Patrick	Tricia, Garrett, Patrick	NA	NA
6.2 Testing Procedures	Patrick	Patrick, Tricia	Tricia	Garrett
7.0 Results & Analysis	Patrick	Tricia	Garrett	Garrett
8.0 Conclusions	Patrick	Tricia, Patrick	Garrett	Garrett
9.0 Recommendations	Garrett	Tricia	Patrick	Patrick
10.0 Global Impact	Tricia	Tricia, Garrett	NA	Patrick
Appendix A	Tricia, Garrett	Tricia, Garrett, Patrick	NA	NA
Appendix B	Garrett	Tricia	NA	NA
Appendix C	Tricia	Tricia	NA	Patrick
Appendix D	Tricia	Tricia, Patrick	NA	NA
Computer Aided Design Drawings	Garrett, Victoria	Garrett, Victoria	NA	Tricia
Drawing of the Hydrofoil	Garrett	Garrett	NA	NA
Drawing of the Frame and Foil Assembly	Garrett	Garrett	NA	NA
Drawing of Crankshaft Link	Victoria	Victoria	NA	Tricia
Drawing of Connecting Link	Victoria	Victoria	NA	Tricia

Table of Contents

Abstract	i
Authorship.....	ii
List of Figures	vii
List of Tables	viii
1. Introduction.....	1
2. Literature Review.....	2
2.1 Renewable Energy Harvesting.....	2
2.1.1 Geothermal.....	2
2.1.2 Solar	3
2.1.3 Wind.....	4
2.1.4 Water	4
2.2 Renewable Energy Applications.....	5
2.3 Energy Generation with Oscillations	6
2.3.1 VIVACE	7
2.3.2 Flapping	8
2.4 Converting Mechanical Energy	11
2.4.1 Piezoelectrics	11
2.4.2 Generators.....	11
2.5 Energy Storage.....	12
2.6 Adaptability and Optimization.....	13
2.6.1 Hydrofoil Geometry.....	13
2.6.2 Power Optimization	15
2.6.3 Fluid Velocity	18
2.6.4 Flapping Actuation.....	19
2.7 Background Summary	20
3. Design Process	21
3.1 Design Intent.....	21
3.2 Design Specifications.....	21
3.2.1 Power Efficiency.....	22
3.2.2 Power Generation.....	23

3.2.3 Frame	25
3.2.4 Hydrofoil.....	26
3.2.5 Hydrofoil Actuation.....	27
4. Calculations.....	28
4.1 Power Calculations	28
4.2 Slider-Crank Mechanism	29
5. Construction.....	32
5.1 Foil	32
5.2 Servo Attachment	33
5.3 Frame	34
5.4 Slider-Crank Mechanism	34
5.5 Servo Actuation Method.....	35
5.6 Assembly.....	36
6. Testing.....	37
6.1 Measurement Systems	37
6.2 Testing Procedure	37
7. Results and Analysis.....	40
8. Conclusions.....	43
9. Recommendations.....	43
10. Global Impact.....	45
10.1 Engineering Ethics	45
10.2 Societal and Global Impact.....	45
10.3 Environmental Impact.....	45
10.4 Codes and Standards	46
10.5 Economic Impact	46
11. References.....	47
12. Appendices.....	51

12.1 Appendix A.....	51
12.2 Appendix B.....	52
12.3 Appendix C.....	53
12.4 Appendix D.....	54
12.5 Appendix E.....	57

List of Figures

Figure 1: Vortex shedding around a stationary cylinder.....	7
Figure 2: Simplified model of the VIVACE device (Bernitsas, 2011).....	8
Figure 3: Schematic diagram of imposed heaving and pitching motions of a flapping wing device (Young et al., 2013)	9
Figure 4: DualWing Generator (Festo, n.d.).....	10
Figure 5: Parameters and basic measurements for an airfoil	14
Figure 6: Feathering parameter of a flapping airfoil; the threshold above which power can be generated (Kinsey & Dumas, 2008).....	17
Figure 7: Navier-Stokes contour plots showing efficiency for combinations of angle of attack and frequency (Kinsey & Dumas, 2008)	18
Figure 8: 3D printed adjustable nozzle for fluid velocity control)	19
Figure 9: Actuation of a flapping hydrofoil at every point in a power generation cycle.....	20
Figure 10: Dimensions of the slider-crank mechanism links in inches	24
Figure 10: The two connecting halves of the 14.40-inch link generation cycle.....	24
Figure 12: The framing system used to form the foil to the correct shape while gluing aluminum to wooden support ribs.....	26
Figures 13 & 14: Free body diagrams showing the forces of water on the hydrofoil and the resulting lift.....	28
Figure 15: Solidworks design of slider-crank mechanism motion	28
Figure 16: Angular velocity of the 6-inch rod about the generator	30
Figure 17: In-progress construction of hydrofoil using aluminum skeleton held in place by support.....	32
Figure 18: Assembled Servo- foil attachment and actuation system.....	32
Figure 19: Solidworks design of servo holder seen fabricated in Figure 15	33
Figure 20: Solidworks model of servo-foil connector shown fabricated in Figure 15	33
Figure 21: Solidworks model of bearing-foil adapter showing bearing seating position and foil rod position	33
Figure 22: Example of MIG weld on steel frame	34

Figure 23: Assembled hydrofoil oscillation system showing fabricated foil, support crossbeam and bearing-rail assembly.	34
Figure 24: Fabricated and assembled slider-crank mechanism showing slider rail, 4-bar linkage, and attachment points	34
Figure 25: Fabricated servo actuation circuit with IR distance sensors.....	35
Figure 26: Waterproof electronics bay for powered systems	35
Figure 27: Completely assembled system with all subsystems attached.....	36
Figure 28: Graph showing frequency versus voltage drop across Thevenin resistor	41
Figure 29: Power output versus frequency of hydrofoil oscillation	41
Figure 30: Complete output of theoretical power calculations.....	51
Figure 31: Graph of 6-inch linkage angular velocity as the foil oscillates	52
Figure 32: Instantaneous power produced by oscillation, varying with time.....	52
Figure 33: Design drawing for modeled NACA0015 foil	57
Figure 34: Design drawing for full Solidworks assembly	58
Figure 35: Design drawing for full crank shaft linkage.....	59
Figure 36: Design drawing for long 4-bar linkage.....	60

List of Tables

Table 1: Weighted design matrix for selection of device	21
Table 2: Scale for weighted design matrix	22
Table 3: Testing plan to find optimal hydrofoil angle of attack	38
Table 4: Example of data collected in dryland testing.....	39
Table 5: Comparison of power ratios calculate at different testing frequencies.....	42
Table 6: Sample data table for 2.0 Hz frequency testing.....	53
Table 7: All test values for 0.67 Hz frequency	54
Table 8: All test values for 1 Hz frequency	55
Table 9: All test values for 2 Hz frequency	56

Chapter 1: Introduction

Producing sustainable, clean energy has long been a pressing challenge for our world. Worldwide energy consumption is expected to rise nearly 50% by the year 2050 (Kahan, 2019), so the need for clean, environmentally friendly energy alternatives has never been greater. Currently, Geothermal, Solar, Wind, and Hydropower make up only 11% of the energy produced by the U.S.A. (Kahan, 2019). This is due to several factors including high startup and maintenance costs, low power density and efficiency compared to natural gas and oil, and dependency on environmental factors such as sunlight or wind. Sustainable energy generation for the future depends on developing consistent and reliable renewable energy harvesting techniques at a comparable cost to natural gas and oil.

Hydropower is one such area with potential for improvement. This method utilizes the energy in flowing water to generate electricity. Hydropower has a key advantage over other common renewable methods since it has a higher power density than wind power, is more reliable than solar power, and is more adaptable than geothermal power. However, current common hydropower methods have several limitations. Hydroelectric dams require large rivers with high volumetric flow to operate effectively. Underwater turbines require streams or tidal areas with a high velocity to turn their blades and produce energy. Additionally, both methods have negative impacts on marine life by destroying habitats, physically harming wildlife, and disrupting the movement of aquatic animals.

To counteract the problems shown in current methods, we have developed a new method utilizing a flapping hydrofoil to harness hydropower. The hydrofoil is attached to two vertical rails and is pitched and heaved underwater by an actuator to produce an oscillating motion perpendicular to the fluid flow. This linear oscillation is captured as energy. Our oscillating hydrofoil design solves several problems present in conventional hydropower. Unlike hydro dams, this device is easily adaptable to small streams and rivers. Contrary to turbines, it can be utilized at velocities as low as 0.1m/s and Reynolds numbers as low as 500 (Kinsey & Dumas, 2008). Additionally, a flapping hydrofoil generator operates efficiently at a low frequency and does not obstruct wildlife movement, making it an environmentally friendly alternative.

Flapping hydrofoil power is a promising alternative to conventional hydropower methods. However, it has several limitations such as high energy cost and low efficiency which impact its viability. Research has been done on optimizing hydrofoils for oscillation in water as

well as determining the optimal frequency of oscillation. More research still needs to be done to determine the optimal hydrofoil material, electrical energy conversion method, and optimal pitch angle for different Reynolds numbers. Additionally, an alternative method for pitching and heaving the hydrofoil has yet to be investigated.

The goal of our project is to build and test a hydrofoil flapping device using a new flapping actuation method, a geometry and weight optimized hydrofoil, and a new electrical current generation method utilizing electromagnetic rails. We will then optimize the frequency, amplitude, pitch angle, and damping of our system to maximize power output.

Chapter 2: Literature Review

The purpose of this literature review is to introduce hydrofoil flapping as a power generation technique and to discuss the optimization of the flapping motion to maximize power. First, our team analyzed and investigated current clean energy generation methods, their limitations, and their current adaptations. Our team then studied the use of oscillation to generate hydropower and investigated current methods such as a Vortex Induced Vibration (VIV) device made by the University of Michigan and discussed its limitations (Bernitsas, Raghavan, Ben-Simon, & Garcia, 2008). We then introduced hydrofoil flapping as an alternative method for hydropower generation and discussed its adaptability, optimization, advantages, and limitations. We also considered altering the amount of flow accessible to the device through flow manipulation. Finally, we researched new methods for electrical current generation from the oscillator and a new method for actuating the hydrofoil to modify the attack angle.

2.1 Renewable Energy Harvesting

Renewable energy harvesting is key to the sustainability of our planet. Fossil fuels contribute to greenhouse gasses, increasing global warming. The energy sources below are alternative methods of energy harvesting implemented to alleviate the effects of greenhouse gasses.

2.1.1 Geothermal

Geothermal energy harnesses the heat found beneath the Earth's surface by converting water to steam. The steam then carries the energy to the surface, which is used to spin turbines

and results in electricity production (Geothermal Energy, 2017). Once the energy from the steam has been used, it is cooled in a cooling tower and pumped back underground.

To be viable for energy production, the source must be in a tectonically active region where the crust is thinner, meaning the Earth is hotter at shallower depths (International Renewable Energy Agency (IRENA), n.d.). One example of this is Iceland, which uses geothermal energy for 30% of its electricity, or about 4 terawatt hours of energy a year (IRENA, n.d.; Runyon, 2020). It is estimated that Iceland has the capacity to produce up to 30 terawatt hours a year (Runyon, 2020).

There are several limitations to geothermal energy. There is a high risk for finding new sources, along with a high initial investment (Lund, 2018). While there is generally a low risk, use of geothermal energy should be avoided in areas with high seismic activity since drilling the wells increases the risk of small earthquakes (National Park Service (NPS), 2020). Additionally, wells can cause the land above to sink if they are not built properly. Building a geothermal plant can cause soil erosion and compaction, along with clearing of trees and wildlife disturbance. The plants themselves can emit harmful gases, which contribute to air pollution and acid rain.

2.1.2 Solar

Solar energy has been steadily increasing in popularity as an alternative renewable energy source to coal and natural gas. A photovoltaic solar panel is the most common method used to convert sunlight to usable energy such as electricity or heat. Photovoltaic panels work by using the sun to create a current between a positively charged plate and a negatively charged plate that are sandwiched together inside the panel (Toothman & Aldous, 2020). When the sunlight hits the positively charged panel, the energy from the sun's photons breaks electrons loose, enabling them to travel towards the negatively charged panel. These electrons are then picked up by electrical contacts that lie between the negative and positive layers and are transferred through an external circuit to create electrical current (Dhar, 2017).

These photovoltaic panels are widely used for water heating and cooling, steam generation, drying and dehydration, and air conditioning systems (Toothman & Aldous, 2020). In all these applications, photovoltaic solar panels are used as a zero-emission alternative to conventional energy generation methods.

Despite having a multitude of useful applications, several disadvantages exist with solar energy generation. On average, sunlight is only available five hours per day, and power production of solar panels is limited to this narrow window (Dhar, 2017). Additionally, even when the panels are actively producing energy, they maintain an efficiency of only 10-20%. High installation and maintenance costs are another major drawback. The average 5kW household solar system costs nearly \$13,000 to install and requires constant cleaning and battery maintenance. Finally, unlike other renewable energy methods such as water generation, solar panel production produces hazardous byproducts such as silicon tetrachloride which is costly to recycle (Toothman & Aldous, 2020).

2.1.3 Wind

Another source of renewable energy is wind. People have been using wind to power various devices for thousands of years (U.S. Energy Information Administration, 2020). Modern wind power mainly falls into two categories; rotating wind turbines and vortex induced vibration models. The most recognizable are the first category, which use the principles of lift and drag to rotate a rotor (Office of Energy Efficiency and Renewable Energy, n.d.). This motion, whether directly or indirectly, turns a generator to produce electricity. Alternatively, some wind power is produced by vortex induced vibrations which typically operate in a linear fashion. This technique involves the principle of vortex shedding which in turn causes oscillation of a bluff body (Diltz, Gagnon, O'Connor, Wedell, 2017).

There are many advantages and disadvantages of using wind to produce electricity (Office of Energy Efficiency and Renewable Energy, n.d.). Some of the advantages include cost-effectiveness and sustainability. Out of the available energy sources today, it is one of the lowest priced at around one to two cents per kilowatt-hour. Some of the disadvantages include noise pollution and wildlife impact. Spinning turbines cause barotrauma and death to birds and bats that fly into them.

2.1.4 Water

The kinetic energy of moving water can be harnessed to generate power. The general concept widely used today is based on water flowing over a turbine or other device that captures

this kinetic energy. The turbine usually powers a generator that uses magnetic induction to generate electricity.

A dam with turbines is the most common method of large-scale hydroelectric power. The dam is used to create a reservoir of water with high potential energy which is converted to kinetic energy when it descends through channels in the dam to turn the turbines. The dam also allows plant engineers to control the flow rate in response to power demands. However, a large dam has environmental consequences. An artificial reservoir can disrupt or destroy wetland ecosystems and communities on the banks of the river. The dam also prevents fish from travelling through the river, and turbines kill fish that pass through the channels.

Another form of hydroelectric power is the smaller scale “micro hydro.” These systems are small enough that they usually do not have a significant negative impact on aquatic life, but they generate substantially less power. Micro-hydro systems are good for powering homes, businesses, or small collections of buildings on their own micro-grids (Energy.gov, n.d.). Due to the low environmental impact of micro-hydro systems and their use on small scales, we decided to focus on this source of renewable energy.

2.2 Renewable Energy Applications

One substantial benefit of renewable energy is its lessened impact on the environment compared to conventional energy sources. However, while the electricity produced through renewables does not contribute the same levels of pollution and greenhouse gasses as traditional non-renewables, it is not without its consequences. Renewable energy impacts the wildlife within the region of production. It is estimated that 50 million acres of land will be developed for energy production, mainly renewables, by the year 2035 (Moore, 2019). This development will require clearing land and building access roads. The impact will vary based on location and energy harvesting method. Lasting impacts on wildlife include physical injury and death to millions of bats and birds each year through collisions with both on and offshore wind turbines. Off-shore turbines also disrupt marine life and ecosystems along the seafloor, including reefs. On-shore turbines produce ambient noise, which negatively impacts local bird populations by reducing their numbers and affecting their behavior. “Power tower” solar plants that concentrate sunlight into beams are hot enough to incinerate birds and insects. Hydroelectric dams prevent

fish from using typical migrating routes, which disrupts breeding and causes high mortality rates among juveniles.

Despite the drawbacks, renewables can provide clean energy to many areas across the world, including remote areas that would not have access to electricity otherwise. Additionally, locals can maintain small scale systems themselves (Sustainia, 2018). For these reasons, renewable energy sources are used in many National Parks for visitor centers, lighting, and offices. Solar energy is a popular energy source for parks, with uses ranging from hot water systems to warehouses and communication centers. The Channel Islands National Park uses wind turbines, a less popular option in parks since they obstruct the scenery and detract from the natural beauty of the parks. Geothermal energy is another less common energy source for national parks. The Santa Monica Mountains National Recreation Area uses geothermal energy for exterior lighting and powering the visitor center. Mesa Verde National Park is among those that use hydropower as an energy source. Along with solar power, their 22kW micro-turbine provides 95% of the energy used in their park buildings (Office of Energy Efficiency & Renewable Energy [OEERE] [C], n.d.; OEERE [E], n.d.). These buildings include a curation facility, visitor center, and office space (OEERE [C] n.d.). One benefit to using renewables within national parks is that many parks are in remote areas where fuel deliveries are costly. Using renewables instead cuts down on this expense. Additionally, using renewables protects Earth, which furthers the purposes of national parks.

Renewable energy can be used on a wide range of scales. Devices range from milliwatts to megawatts (Karow, 2019; “Renewable Energy: Utility Scale,” n.d.). Individual households can have their own systems, or they can be a part of a utility-scale system. To qualify as a utility-scale system, the renewables must produce 10 MW or more (OEERE [D], n.d.). These systems include solar, wind, geothermal, and hydropower (Farrell, 2018; OEERE [E], n.d.; Bureau of Reclamation, 2018).

2.3 Energy Generation with Oscillations

While most energy is harvested by various devices that use fluid flow to rotate, this is not the only way to harness power from fluid. There are also methods of harnessing energy through oscillation, which is a linear back and forth movement. These methods have lower noise and wildlife impacts because of lower foil velocities (Young et. al, 2014). They also have the

potential to be more effective in shallow water and small-scale operations which is ideal for our application of national park streams. Vortex induced vibrations and flapping are two forms of oscillation which are used for energy generation.

2.3.1 VIVACE

One method for harnessing energy with oscillation is by amplifying the phenomenon known as Vortex Induced Vibrations (VIV). VIV is created by a vortex shedding around the cylindrical body as shown in Figure 1. This creates a repeating pattern of high- and low-pressure swirling vortices known as a Karman vortex street (Ericsson, 2012). The imbalance between the low- and high-pressure zones creates force on the cylinder perpendicular to the fluid flow which, if not opposed, causes the cylinder to accelerate either up or down. Springs with a natural frequency close to the frequency of oscillation are attached to either end of the body. These springs will then constructively combine with the VIV to increase amplitude of oscillation. By enhancing, rather than spoiling this oscillating motion, VIV can be used to harness power from a stream at low fluid velocities.

The Vortex Induced Vibration Aquatic Clean Energy (VIVACE) device exploits the natural phenomenon of vortex induced vibrations to harness energy from water streams as slow as 0.25 m/s with low or no head (Bernitsas, Raghavan, Ben-Simon, & Garcia, 2008). This device is being developed to be used as a fish friendly alternative to water turbines and dams by harnessing energy at very low frequencies, around 1Hz, while still allowing passage of wildlife in and around the device (Bernitsas, Raghavan, Ben-Simon, & Garcia, 2008).

Some limitations exist for the VIVACE device that make it unsuitable for our application. Firstly, synchronizing the device with changing fluid flow to maintain VIV has proved to be a challenge in tests on the ocean floor due to the need to match the natural

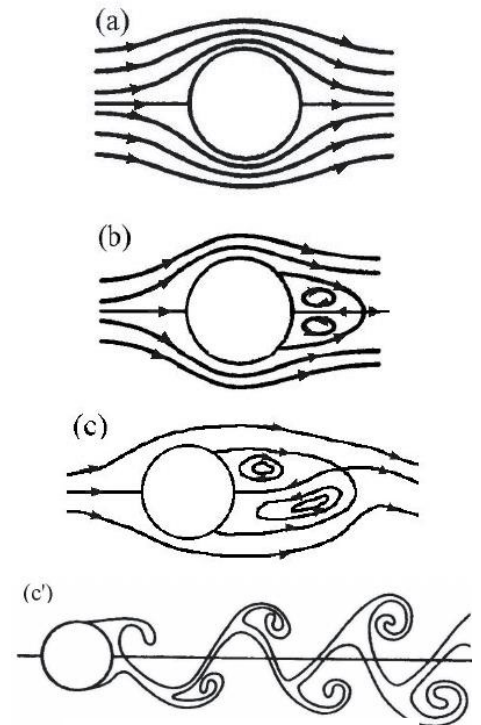


Figure 1: Vortex shedding around a stationary cylinder

frequency of the spring to the VIV frequency (Ben-Simon, Raghavan, & Garcia, 2009). This may prove to be an even greater challenge for small rivers where fluid velocities are expected to change more dramatically. Secondly, due to the complexity of synchronizing the motion of the cylinder with fluid flow, it may be impractical to use in a remote area such as a national park where a system failure would be difficult to diagnose without an expert. Finally, on smaller scales such as our application, VIVACE has a relatively high complexity compared to its power output (Bernitsas, Ben-Simon, Raghavan, & Garcia, 2008). To address these problems, our team investigated a similar alternative which utilizes a flapping airfoil to generate power.

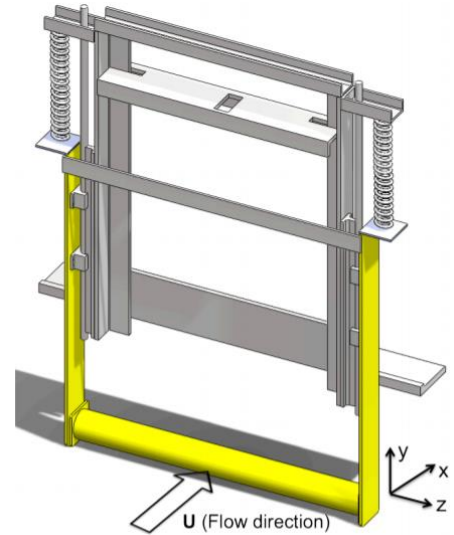


Figure 2: Simplified model of the VIVACE device (Bernitsas, 2011)

2.3.2 Flapping

The goal of our project is to generate electricity simply and effectively from low velocity streams for national parks. Our project draws inspiration from the linear oscillations of VIV without the complexity. By using a flapping hydrofoil rather than VIV or a rotating turbine, our project will benefit from simplicity and higher lifts than otherwise achievable through rotating turbines.

Similar to VIV devices, flapping foils can produce energy efficiently at low fluid velocities, unlike conventional turbines (Young et. al, 2014). Additionally, flapping foil power oscillates at a similar frequency to a VIV device which makes it safer for wildlife. Unlike VIV devices, flapping foils are much more easily suited to operate over a large range of fluid velocities like those seen in rivers.

Motion

Flapping motion is created by cyclically angling an airfoil upwards and downwards. This allows fluid to push the foil up and down creating an oscillating motion that can be described using Equations 1 and 2:

$$\theta(t) = \theta_0 \sin(\gamma t) \quad (1)$$

$$h(t) = H_0 \sin(\gamma t + \varphi) \quad (2)$$

where θ_0 and H_0 represent the amplitude of pitching and heaving, respectively. γ is the angular frequency and ϕ is the phase angle difference between the motions. These parameters are shown in Figure 3:

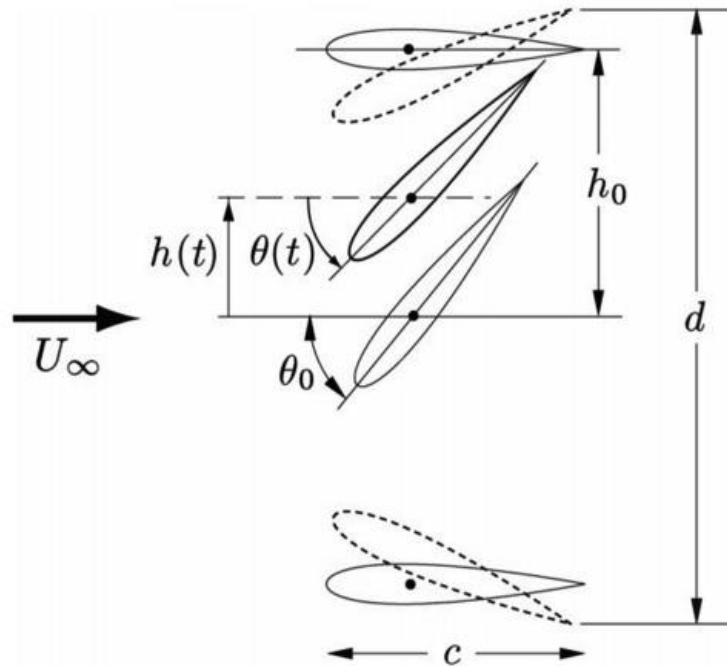


Figure 3: Schematic diagram of imposed heaving and pitching motions of a flapping wing device (Young et al., 2013)

Flapping foils can also use leading edge vortices (LEV) to create high instantaneous vertical forces which increase the power available for harnessing. LEV is caused by separation of flow at the leading edge which produces low pressures in the vortex core. This low-pressure zone increases as the angle of attack of the foil increases, which generates additional lift.

At a smaller scale, flapping winged vehicles are more beneficial than fixed wing vehicles due to the low efficiencies of fixed wing vehicle propellers. Flapping winged vehicles have a higher induced lift than stationary airfoils, and they require less power to operate at smaller scales (Sachs, 2016). Additionally, flapping airfoils have better efficiency than rotary turbines when the incoming water velocity drops (Liu et. al, 2017). This is beneficial to our project because streams do not have constant flows throughout the year. With improved efficiency at lower velocity, our project should work well in stream conditions. Overall, flapping airfoils work well on small scales (Sullivan, 2014).

Energy Generation

To generate electricity, the axes of the airfoils are connected to rails that convert the linear motion of the foil to rotational motion, generating electricity. This can be seen in the DualWing Generator by Festo which utilizes a series of belts and pulleys to transfer the linear vertical motion to a rotational generator (Festo, n.d.). The DualWing Generator can produce



Figure 4: DualWing Generator (Festo, n.d.)

between 50 and 200 W/m² at wind speeds from 4 to 12 m/s. While streams have velocities between 1 and 3 m/s, they have much more power per area than wind because of the higher density. In fact, water moving at 3 m/s is equivalent in force per area to an EF5 tornado, or about 89 m/s (Ballisty, 2015). Generator by Festo which utilizes a series of belts and pulleys to transfer the linear vertical motion to a rotational generator (Festo, n.d.). The DualWing Generator can produce between 50 and 200 W/m² at wind speeds from 4 to 12 m/s. While streams have velocities between 1 and 3 m/s, they have much more power per area than wind because of the higher density. In fact, water moving at 3 m/s is equivalent in force per area to an EF5 tornado, or about 89 m/s (Ballisty, 2015).

The power density of air and water can be compared using Equation 3:

$$P = \frac{1}{2} \rho A U_{\infty}^3 \quad (3)$$

where P is the power produce, ρ is the density of the fluid, A is area of the foil perpendicular to the fluid and U_{∞} is the stream velocity. Comparing identical foils in air and water, we can

eliminate area from the equation. Substituting a wind speed of 8 m/s and a water speed of 2 m/s we calculated the following:

$$P_{Wind} = \frac{1}{2} (1.2754 \frac{kg}{m^3}) (8 \frac{m}{s})^3 = 326.5 \frac{W}{m^2}$$

$$P_{Water} = \frac{1}{2} (998 \frac{kg}{m^3}) (2 \frac{m}{s})^3 = 3992.0 \frac{W}{m^2}$$

These results showcase the benefit of water's high density for power generation. Therefore, due to the higher potential for power generation at the lower velocities available in water, our team decided to use water, instead of wind, as the energizing fluid in our project.

Challenges of using a hydrofoil in water rather than an airfoil in air are the increased friction and increased force needed to reposition the foil's angle. However, since water has such a higher power density than air, we will work to overcome these obstacles.

2.4 Converting Mechanical Energy

2.4.1 Piezoelectrics

The piezoelectric effect is that certain materials produce an electrical field when put under mechanical stress. This occurs because the stress aligns positive and negative charge centers, allowing for a flow of charge (Nanomotion, 2018). This effect is reversible, meaning that applying electrical charges to the material causes a mechanical stress. Piezoelectrics do not produce high volumes of power. For example, a system that incorporates piezoelectrics into flags produces milliwatts of power as the flags flap in the wind (Karow, 2019). While piezoelectrics can be used to charge batteries, there is still a significant difference between the capabilities of current technology and its potential.

2.4.2 Generators

Most of the electricity used by consumers is produced by rotating generators (U.S. Energy Information Administration, 2019). These devices use the principles of magnetism and electricity to convert forms of energy into electricity we can use. An electrical current is produced when a magnet is moved inside of or around a coil of wires. Today, most generators use an electromagnet instead of a traditional magnet. Electromagnets are magnetic fields that are produced by electricity. The most common configuration is to have a rotating electromagnetic

shaft surrounding sections of wire coils. When the shaft rotates, the wire coils produce electric current.

In addition to the traditional rotary generators, there are also linear generators which are commonly used adjacent to various types of engines (Arof, Wijono, Nor, 2005). These generators operate on the same principles as the rotary variety except in relation to motion. A magnet is moved linearly back and forth inside or next to a coil of wire. Linear generators experience an end effect, where the motion stops and reverses, while rotary generators never reach an endpoint in motion. Despite operating along different paths while generating energy, both linear and rotational generators successfully produce electricity and share the same energy storage solutions.

2.5 Energy Storage

A problem of equal importance to harnessing and generating energy is how to store excess energy for use during lower production times. Energy produced by renewable sources can be stored in several ways, most commonly as potential energy. A hydroelectric dam does this by creating a reservoir of water above the turbines. Another form of potential energy storage is filling a tank with compressed air. Excess energy can be used to compress the air, and when it is needed, electricity can be generated by releasing it.

Another common energy storage solution exists in batteries. Batteries are made up of electrochemical cells; chemical reactions that generate electrical potential when active. This usually takes the form of two electrodes immersed in an electrolyte solution. Two common types are lead-acid batteries, which are commonly used in cars, and lithium-ion batteries, the main type used in consumer electronics such as cell phones. When power is applied to the battery, it causes the reverse reaction, allowing the energy to be stored. The battery can then discharge this energy through the forward reaction at a later time.

Energy can also be stored in the form of fuels. For example, a tank of gasoline or propane can be seen as a container of potential energy. The disadvantage of this type of storage is that many of these fuels are not renewable. Releasing the energy requires burning them, which can negatively impact the environment. Both batteries and fuels can be classified as chemical energy storage, as the energy is released by a chemical reaction. Thus, development and improvement of new energy storage methods of these forms is often a chemical engineering problem. Batteries

are mass produced, making common types of them cheap and easy to acquire. Using a battery eliminates the need to design a more complex energy storage system.

2.6 Adaptability and Optimization

To maximize the potential of any energy generation device, we must successfully adapt the device to different environments and conditions and optimize the device to maximize the power output. To understand how to achieve a maximum power output, we must first understand how power is defined, how power is extracted from flapping, and which parameters affect how much power is produced.

2.6.1 Hydrofoil Geometry

Hydrofoils have specialized terms for their dimensions (Benson, 2014). The leading edge of a foil is the first part to interact with the flow. The trailing edge is the last to interact with the flow. The chord is the width of the foil from the leading edge to the trailing edge and the imaginary line this creates is called the chord line. The span is the length of the foil. From a top view, the span is seen left to right. The aspect ratio of a foil is the ratio of the span to the chord, $\frac{s}{c}$. The camber of the foil is the maximum distance between the chord line and the top of the foil. The mean camber line is a curve that follows the halfway points between the upper and lower surfaces of the foil. These dimensions along with the anhedral angle are shown in the diagram below.

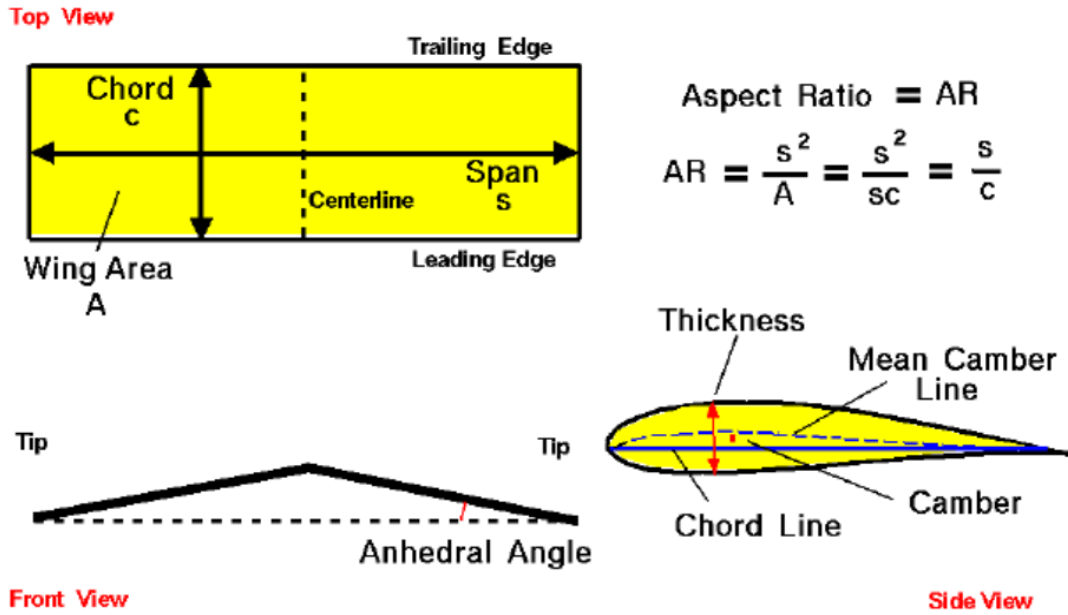


Figure 5: Parameters and basic measurements for an airfoil

The first step in determining hydrofoil dimensions is to define the flow of fluid around the foil. One of the parameters used to determine the free surface flow over the hydrofoil is the Froude number (Wilson, 1978). The Froude number is a dimensionless factor that indicates the influence of gravity on the fluid's motion (The Editors of Encyclopedia Britannica, 2016). The equation for the general Froude number is shown below:

$$Fr = \frac{v}{\sqrt{gd}} \quad (4)$$

where d = depth of flow, g = gravitational acceleration, v = celerity of small surface (or gravity) waves, and Fr = Froude number.

When $Fr < 1$ small surface waves can move upstream. When $Fr > 1$ small surface waves go downstream. The critical Froude number is when $Fr = 1$ which indicates that the velocity of flow equals the velocity of the surface waves. To further characterize the fluid flow over the specific dimensions of the hydrofoil, equations are used to determine the chord, depth, and half-span Froude numbers as shown below:

$$\text{Chord Froude Number: } F_c = \frac{U}{\sqrt{gc_a}} \quad (5)$$

$$\text{Depth Froude Number: } F_d = \frac{U}{\sqrt{gd}} = F_c \sqrt{\frac{2}{A}} \quad (6)$$

$$\text{Half-span Froude Number: } F_b = \frac{U}{\sqrt{gb}} = F_c \sqrt{\frac{2}{A}} \quad (7)$$

To be fully useful, the Froude number must be used along with the relative depth of submergence to fully characterize the free surface flow.

Once fluid flow is defined, parameters can be selected which optimize the lift and minimize the drag on a foil. Kinsey & Dumas found the chord length of a flapping hydrofoil should be approximately equal to half of the heaving amplitude. To further maximize system efficiency, the aspect ratio should be maximized (Cutler, 2015).

Most flapping hydrofoil designs utilize a symmetric hydrofoil, such as a NACA0015 foil, so that the forces created by pitching and heaving are equal. This enables similar power generation from both up and down cycles.

In order to be effective at flapping while submerged in water, the hydrofoil must either be neutrally buoyant, where the weight of the displaced fluid equals the weight of the foil, or negatively buoyant, where the weight of the displaced fluid is less than the weight of the foil. This will enable the foil to produce lift in the flow of water. Proper weight can be achieved through controlling the buoyancy. As Archimedes' principle states, "the buoyant force on an object is equal to the weight of the fluid displaced by the object" (Khan Academy, 2020). A useful variation of this principle is the buoyant force equals the volume of the fluid displaced, V_f , times the density, ρ , and gravitational acceleration, g , as shown below:

$$F_{buoyant} = \rho g V_f \quad (8)$$

This variation of the equation is useful for determining the weight of a submerged hydrofoil. Once the buoyancy and optimal geometry of the hydrofoil have been determined, power optimization can be analyzed.

2.6.2 Power Optimization

Power Definition

Hydrofoil flapping generates power by creating oscillating, vertical motion. This motion is described as heaving, or plunging, and pitching, or climbing. Calculating the power density of this motion, by modifying Equation 9, determines the amount of power available for harvesting:

$$P_t = \frac{1}{2} \rho U^3 \infty d \quad (9)$$

where U_∞ is the stream velocity, ρ is the density of the free stream fluid, and h is amplitude of oscillation (Lee & Bernitsas, 2011). P_t represents the total amount of power available. The actual average power produced over a cycle is determined by the mean power contributed by the heaving motion and the power extracted from the pitching motion (Kinsey & Dumas, 2008). Hence, the mean power over a cycle can be defined as:

$$P = P_p + P_h \quad (10)$$

where P_p is the power produced by pitching and P_h is the power extracted from heaving. From Equations 9 and 10, the efficiency of the hydrofoil can be determined by comparing the power extracted to the power available as shown in Equation 11:

$$\eta = \frac{P}{P_t} = \frac{P_p + P_h}{\frac{1}{2}\rho U_\infty^3 h} \quad (11)$$

where the efficiency of a flapping foil is shown to be the total power produced by pitching and heaving to the total power available for harvesting (Zhu, Zhang, & Huang, 2019).

Power Regimes

Operating within the power regime maximizes power output and efficiency. A power regime is the region where the angle of attack and frequency of a flapping hydrofoil combine to produce power. This is determined by the angle of attack, θ_0 . By optimizing θ_0 , the oscillation frequency can be maximized while maintaining a maximum amplitude which is optimal for maximum power output. The optimal angle of attack can be found by defining the regime where a hydrofoil will produce power. This regime is determined by a feathering parameter given by:

$$X = \frac{\theta_0}{\tan^{-1}(hc\omega U_\infty)} \quad (12)$$

where h is the plunge amplitude, c is the chord length, and ω is the angular frequency (Young, Lai, & Platzer, 2014). When $X = 1$, the mean power extracted over one cycle is nearly zero. The power extraction region exists when $X > 1$.

Power Extraction

From Equation 9, it can be determined that the power extraction of a given hydrofoil can be optimized by modifying angle of attack, the plunge amplitude, the angular frequency, and the fluid velocity. Defining the non-dimensional frequency shown in Equation 13 relates these parameters:

$$f^* = \frac{fc}{U_\infty} \quad (13)$$

where f is the frequency of oscillation, c is the chord, and U_∞ is stream velocity. Using a dimensionless frequency allows variation of one parameter rather than all three that contribute to frequency. This can be used to optimize power output more easily. This dimensionless frequency determines the minimum angle of attack needed for effective power generation at each different $X = 1$, by using Figure 6. The solid line represents $X > 1$ the transition between the propulsion and power regions for the hydrofoil. Above the line $X > 1$ is the region where the hydrofoil will produce power.

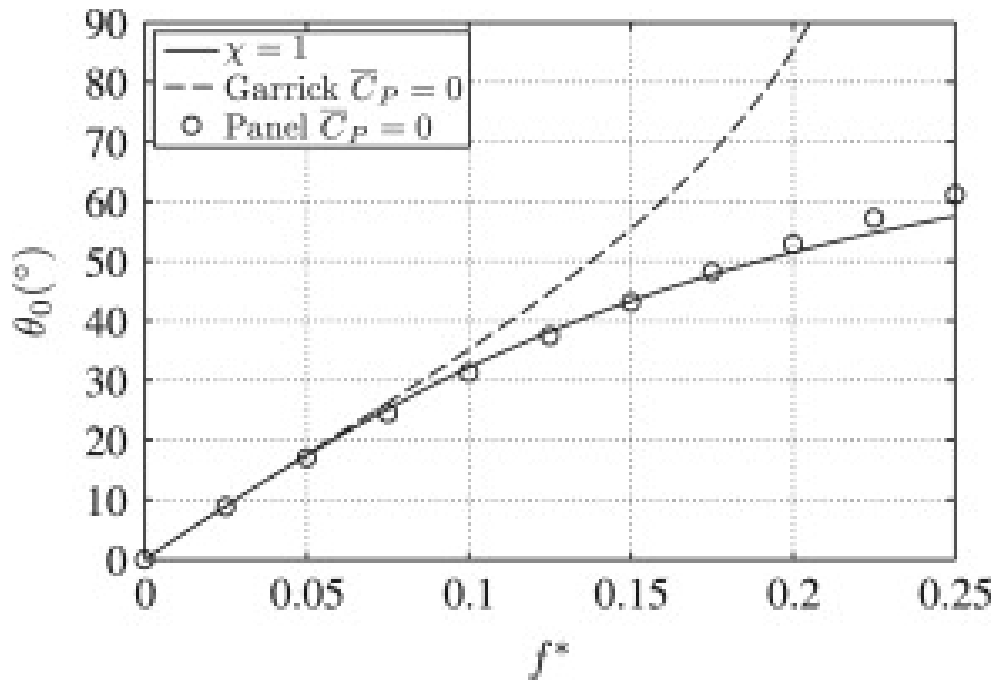


Figure 6: Feathering parameter of a flapping airfoil; the threshold above which power can be generated (Kinsey & Dumas, 2008)

Power Efficiency Optimization

The efficiency at every point in the power region has been estimated by Kinsey & Dumas (2008) using a National Advisory Committee for Aeronautics (NACA) 0015 hydrofoil. Navier-Stokes efficiency contours were generated from a parametric study. Figure 7 shows the contour plot which has a maximum efficiency of around 35% at a $\theta_0 = 75^\circ$ Stokes $f^* = 0.15$ and [OB] . This makes it very competitive with other clean energy generation methods discussed in our literature review. Similar studies have been conducted by Zhu (2011) and Platzer et al. (2009) with modified hydrofoil geometry and flow parameters with both studies yielding similar results.

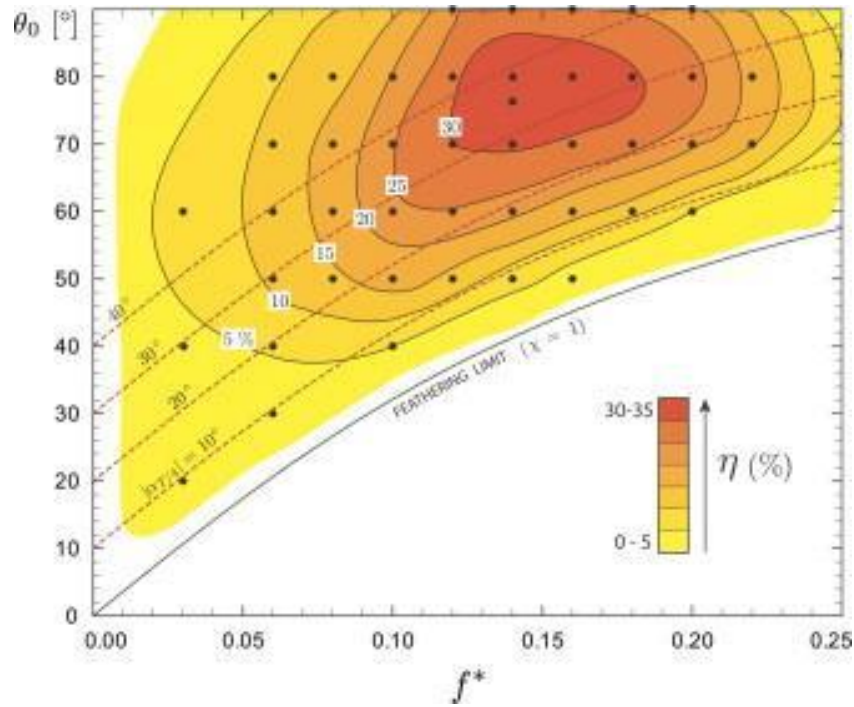


Figure 7: Navier-Stokes contour plots showing efficiency for combinations of angle of attack and frequency (Kinsey & Dumas, 2008)

2.6.3 Fluid Velocity

One way to adjust the dimensionless frequency of oscillation to optimize the power generated is through fluid velocity manipulation. This can be done by varying the cross-sectional area of an intake device. Due to conservation of flow, the velocity of the fluid will increase when the area is decreased so flow rate is maintained. This means the following equations are true:

$$Q_1 = Q_2 \quad (14)$$

$$Q = vA \quad (15)$$

$$v_1A_1 = v_2A_2 \quad (16)$$

where Q is the volumetric flow rate, v is the velocity, and A is the cross-sectional area. If the area is decreased by a certain factor, the velocity will increase by the same factor. In a system with a circular cross section, πr^2 can be substituted for A . When π is factored out, the following relation is true:

$$v_1 r_1^2 = v_2 r_2^2 \quad (17)$$

This means that the velocity is inversely proportional to the square of the radius.

A common method of adjusting the cross-sectional area is with a variable area nozzle like the ones found on aircraft afterburners. A small-scale example of such a device is shown below:

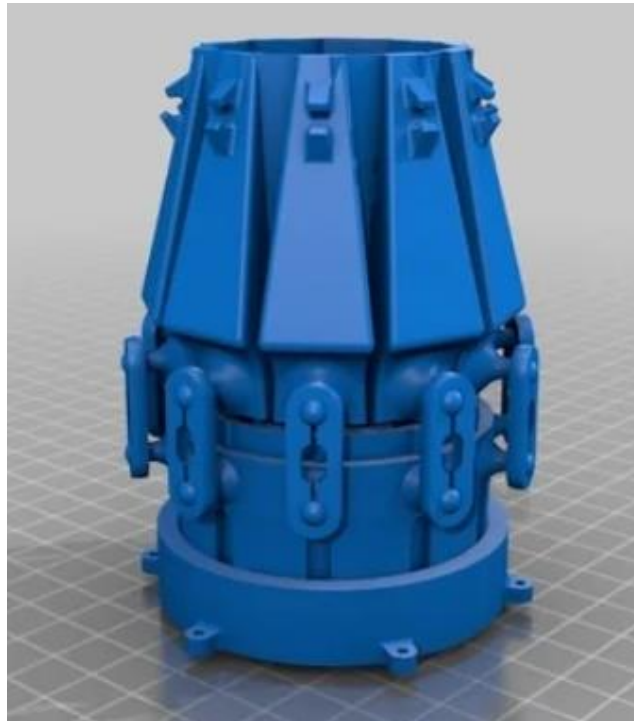


Figure 8: 3D printed adjustable nozzle for fluid velocity control)

Using this design, the minimum radius is half of the maximum radius, meaning the maximum velocity is 4 times the minimum.

Another simple system is a rectangular channel with adjustable walls. They can be angled inward toward the aperture, decreasing the cross-sectional area. In this case, the area is equal to the height times the width, which means the area, and thus velocity, changes in a linear fashion when the width is adjusted. Either of these methods could be used to vary the water velocity to optimize power generation in our device.

2.6.4 Flapping Actuation

The force needed to actuate and hold the flap is relatively small since the hydrofoil is nearly balanced on its axis of rotation as shown in Figures 3 and 9. However, the force needed for actuation will have to be large enough to overcome both the static forces and the force of the fluid due to virtual mass displacement. The static force from the water will nearly balance around the axis of rotation making the force needed to hold the angle small as shown in Equation 18.

$$M_{B,Water} - M_{T,Water} = M_{Hold} \quad (18)$$

$$M_{B,Water} \approx M_{T,Water} \rightarrow M_{Hold} \approx 0$$

The force needed to actuate the foil must overcome both the static forces present as well as the force present from the virtual water mass that the foil will be displacing. The virtual mass

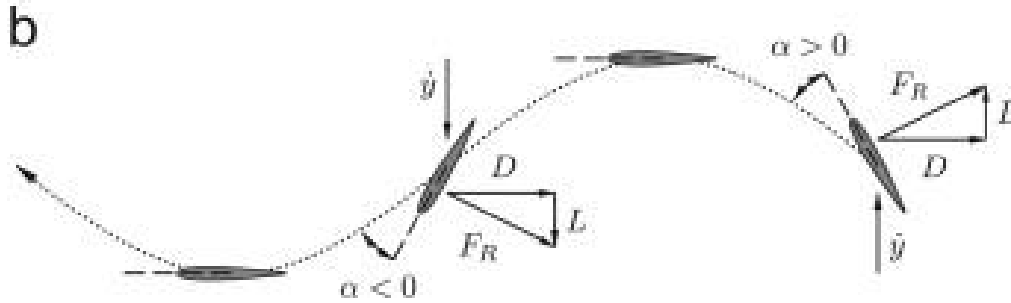


Figure 9: Actuation of a flapping hydrofoil at every point in a power generation cycle

of the water the foil will be displacing can be roughly estimated by finding the total mass of water displaced by the foil and using gravity to find its force on the foil. We used this as a conservative estimate in our design.

2.7 Background Summary

Finding new ways to harness renewable energy has been an ever-growing industry. Alignment with environmental values and accessibility in remote areas makes renewables an enticing choice for power generation within national parks. However, while they reduce carbon emissions, renewable energy methods have negatively impacted wildlife by occupying and obstructing areas that were once habitats for both land animals and aquatic life. While smaller scale systems reduce these effects, existing methods tend to be complex. To counteract these problems, an alternative method utilizing an oscillating foil can be used to generate power. This device harnesses energy from low velocity streams such as those found in many national parks to create electrical current without obstructing or harming wildlife.

Chapter 3: Design Process

3.1 Design intent

Our design intent was to test the concept of oscillating foils in water rather than air, on a smaller scale. This system can be used to generate renewable and consistent power by national parks or individuals in rural areas to provide auxiliary power. Our non-conventional method of oscillation for power generation minimizes possible negative effects on wildlife and maintains beautiful views. We optimized our design for use in a rural stream in Massachusetts to simulate a national park stream. By modifying the angle of attack and the actuation method of our hydrofoil, we maximized power output over a range of fluid velocities.

3.2 Design Specifications

In choosing our design, our team determined optimal parameters for our device to balance affordability, manufacturability and performance. The main parameters we focused on were frame size and construction, hydrofoil geometry, system durability, hydrofoil actuation system, and power generation system. To help us choose an optimal design, we created a weighted matrix to include each of these parameters and used the requirements for our design to pick an optimal configuration. Desirable designs are reliable to ensure a testable prototype, cost effective, and buildable within COVID 19 restrictions.

Design Matrix									
	Weighted Value	Symmetrical Foil, Linear Generator, Electrical Actuation	Symmetrical Foil, Linear Generator, Mechanical Actuation	Symmetrical Foil, Rotational Generator, Electrical Actuation	Symmetrical Foil, Rotational Generator, Mechanical Actuation	Asymmetrical Foil, Linear Generator, Electrical Actuation	Asymmetrical Foil, Linear Generator, Mechanical Actuation	Asymmetrical Foil, Rotational Generator, Electrical Actuation	Asymmetrical Foil, Rotational Generator, Mechanical Actuation
Generates Electricity	0.9	4	5	4	4	4	2	3	4
Time Constraints (3 Terms)	0.8	5	2	4	3	4	2	3	2
Manufacturability in COVID	0.7	3	1	4	2	2	1	3	2
Produces max	0.9	4	4	4	4	2	2	2	2

power throughout full cycle									
Expense of Actuation Method	0.4	3	4	3	4	3	4	3	4
Reliability of Actuation Method	0.9	5	2	5	2	5	2	5	2
Simplicity of Actuation Method	0.5	4	3	4	3	4	3	4	3
Expense of Generation Method	0.8	1	1	4	4	1	1	4	4
Simplicity of Generation Method	0.5	4	4	3	3	4	4	3	3
Totals		23.8	18.1	25.6	20.6	20.5	13.6	21.4	18.0

Table 1: Weighted design matrix for selection of device

Scale	
5	Desirable
4	
3	Somewhat Desirable
2	
1	Undesirable

Table 2: Scale for weighted design matrix

From this matrix, clearly the superior option contains a symmetrical hydrofoil, rotational generator, and an electrical actuation system.

3.2.1 Power Efficiency

We focused on optimizing the mechanical aspects of our system to maximize energy production. Further parameters contributing to power efficiency include method of actuation and minimizing energy loss from interactions between the frame and foil. Optimizing these parameters enabled us to enhance our power generation.

3.2.2 Power Generation

Harnessing the power from our oscillating hydrofoil was a key consideration for our team. Since the volume of power that a piezoelectric can harness is significantly smaller than the power of a flapping hydrofoil, we did not use it in our design. Our two main options were to harness the linear motion directly using a linear generator, or to use a linkage to transform the linear oscillation into rotational motion to power a conventional generator. Since we are interested in energy harnessing through oscillation, a linear generator would eliminate the need for any gear chain to convert linear oscillations to rotational motion which could decrease efficiency of our device. However, based on our design matrix, we chose to use a slider-crank mechanism to convert linear to rotational motion. Our team chose a 10W high-torque generator to be used in testing along with a custom design and optimized slider-crank mechanism to transfer power.

The slider-crank mechanism we designed transfers the linear motion of the hydrofoil into rotational motion to turn the generator. Grashof's Law states that if the sum of the shortest and longest links is less than the sum of the two other links then at least one link will be able to make a full 360-degree rotation. We used this condition to ensure the link connecting to the generator would be able to complete a full rotation. This was important to us because we wanted to run the generator in one direction since stopping and starting in the opposite direction would be less efficient. Our second longest link in our mechanism is the guiding link, the 12-inch rail the foil oscillates on. We based the lengths of the crankshaft and connecting rod around this value. Figure 10 shows the configuration of the links. Link 1, depicted in red, is the crankshaft and is attached to our generator. Link 2, depicted in green, is the connecting link between the crankshaft and linearly moving bearing of the foil.

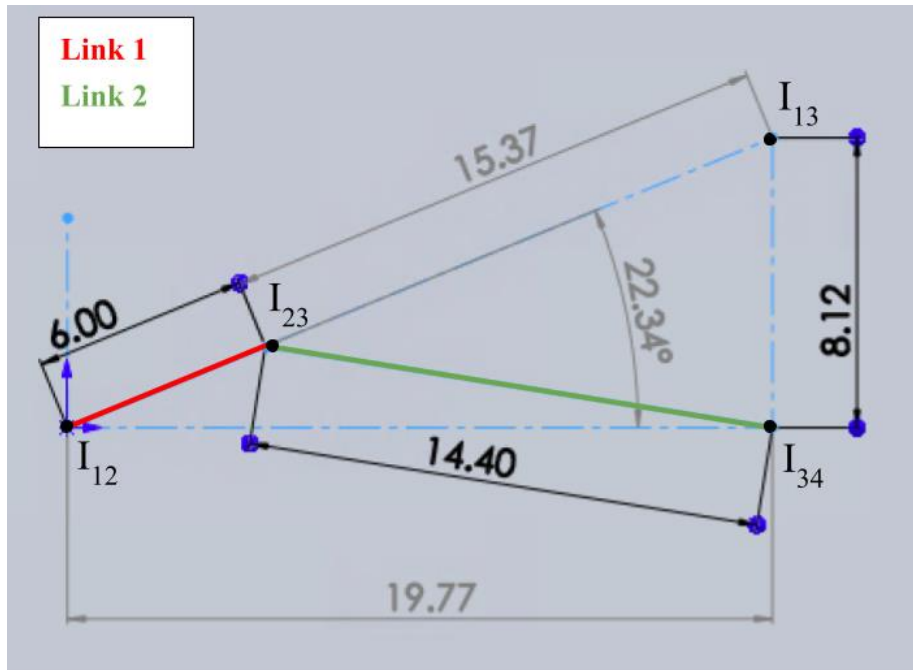


Figure 10: Dimensions of the slider-crank mechanism links in inches

As shown above, the crankshaft is 6 inches, and the connecting link is 14.40 inches. Since these links are unique from products on the market, we chose to fabricate them out of PLA using fused

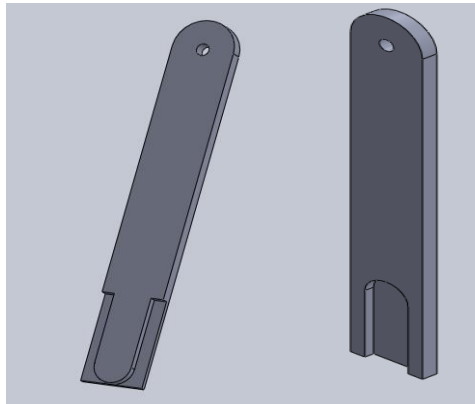


Figure 11: The two connecting halves of the 14.40-inch link generation cycle

deposition modelling. The 14.40-inch link was too long for the print bed, so we designed it for construction by adding a simple tongue and groove. This connects the halves while allowing for resistance when turning since we did not want the connection point to fail. This connection can be seen in Figure 11. Additionally, the link connecting to the shaft of the generator has one hole

that is smaller so there will be an interference fit between the link and the shaft. Once we determined our method for power generation, we developed a frame to contain our system.

3.2.3 Frame

The constraints for our frame were size, waterproofing, durability and portability. Due to the nature of our project, our device needed to be small enough to fit into a car for transportation and light enough to be easily maneuverable between school and testing locations. To fit both these constraints, our team designed a box frame with dimensions 26" x 22" x 5" (L x H x W). Our frame was constructed using a steel L-beam skeleton, giving it a very rigid yet light quality.

While our device does not need to be frictionless, it would be beneficial to limit any excess friction such as that caused by corrosion. To minimize corrosion on power-producing parts of our frame, our team chose to construct our vertical power rails from 316 stainless steel. 316 stainless steel possesses a high corrosion resistance due to its high chrome content and will allow for our linear bearings to smoothly oscillate without increased friction due to corrosion.

In analysis we calculated that our frame would endure a maximum bending stress from the passing water of 1.9 MPa, much less than the approximate max shear stress of 1095 steel which is 350 MPa. This was calculated under the conditions that the bottom of the frame is fixed. Forces on frame from the water were calculated using the Equation 19:

$$F = \frac{C_d A \rho V^2}{2} \quad (19)$$

where A is area, ρ is density of the water, V is velocity of the water, and C_d is a drag coefficient for a rectangular plate like the cross section of the frame perpendicular to the water flow. Based on the ratio of length to width for the frame components, C_d was approximately 1.6. The forces on the were then used to calculate deflection and stress in a similar manner to a cantilever beam, using Equation 20:

$$\sigma = \frac{yFL}{I} \quad (20)$$

where y is the distance to the beam's neutral axis, L is its length, and I is the area moment of inertia. Thus, our frame is significantly stronger than the forces it encounters while submerged under water.

3.2.4 Hydrofoil

In selecting our hydrofoil, our team considered three parameters: weight, shape, and cost. Proper weight can be achieved through controlling the buoyancy. The goal was to have as close to a neutrally buoyant foil as possible. We were concerned the foil would float, and therefore be unable to oscillate. If the foil could not be exactly neutrally buoyant, we wanted it to be slightly negatively buoyant. Therefore, we needed the density of our foil to be $997 \frac{kg}{m^3}$ or greater. With a volume of $0.0012 m^3$, this means the mass needed to be 1.089 kg or greater since $mass = density * volume$.

Our team investigated several different materials for use in constructing our hydrofoil based on the following: density, strength, cost, and machinability. To determine the optimal material, we looked at several common materials used in airfoils both on a hobbyist and professional level. Wood is a very common material for airfoils due to its low cost, good strength, and ease of fabrication. However, wood is not very dense and would require additional weight to be neutrally buoyant. We also investigated metal, but difficulty with fabrication makes it a time-consuming choice. Finally, we researched the use of foam concrete. Foam concrete is cheap, high in strength, and can be easily formed to a specific shape. Additionally, its density can be varied between $400 \frac{kg}{m^3}$ and $1600 \frac{kg}{m^3}$ making it ideal perfect as a neutrally buoyant material in water which has a density of $998 \frac{kg}{m^3}$.

To determine if foam concrete could withstand the bending forces it would need to undergo, our team calculated the maximum bending and shear stress that our airfoil would see. Assuming the airfoil was perpendicular to the stream, we used $v = 3 \frac{m}{s}$, to calculate the force on the airfoil as follows:

$$F_{Foil} = \rho_{water} A_{Foil} v^2 = (998 \frac{kg}{m^3})(0.0232m^2)(3 \frac{m}{s})^2 = 208N \quad (27)$$

We then estimated this force to be roughly at the center of the airfoil and calculated the maximum bending and shear stress on the foil using the following:



Figure 12: The framing system used to form the foil to the correct shape while gluing aluminum to wooden support ribs

$$\sigma_{MAX} = \frac{M_{MAX}y}{I} \quad (21)$$

$$\tau_{MAX} = \frac{V_{MAX}}{A_{xc}} \quad (22)$$

Using Equations 21 and 22 and substituting in roughly estimated values for inertia I and cross-sectional area A_{xc} , we found that $\tau_{MAX} = 02kPa$ and $\sigma_{MAX} = 27kPa$. These values are much less than the maximum shear and bending stress of full-strength concrete so we believe foam concrete will work for our hydrofoil. Due to the continued restrictions in place in response to COVID-19, our team chose to design an airfoil that could be constructed with common hand tools, without the need for access to on campus facilities.

Unfortunately, again due to COVID-19, foam concrete was not a feasible option for us due to the facilities required being unavailable. Instead, we constructed our hydrofoil using wood, aluminum, and regular concrete. While the internal material is not homogeneous, it was distributed in a balanced manner.

After determining the material and buoyancy of our foil, we developed our desired foil shape. For our flapping motion, we wanted to equalize the power produced during the pitching cycle and the heaving cycle. Therefore, we needed an airfoil that would act the same traveling upwards and downwards. We chose the symmetrical NACA 0015 foil for this reason.

This can be accomplished in part by optimizing the aspect ratio of the foil to maximize efficiency. Due to portability and testing limitations, our maximum span possible was 12 inches, giving us an aspect ratio of 4:1. We then determined an amplitude for our oscillator based on the average depth of a stream in Massachusetts which is approximately 0.32 meters, or about 12.5 inches (Bent & Waite, 2013). To maximize the possible amplitude while ensuring maintained submersion of our foil, we chose an amplitude of 12 inches. Based on this, our chord length is 6 inches.

3.2.5 Hydrofoil Actuation

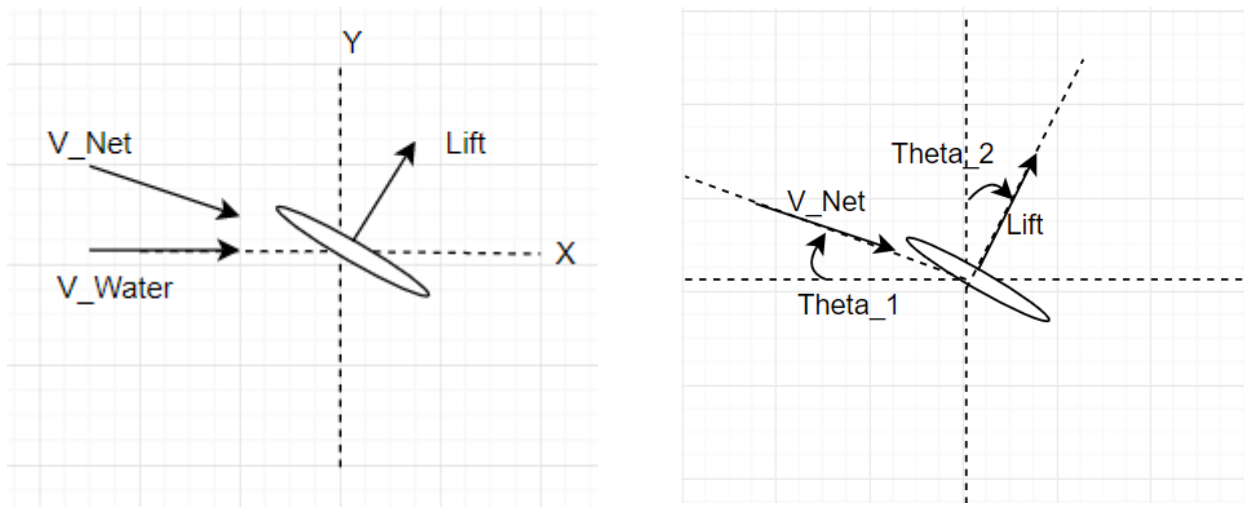
Once we optimized the amount of energy we can harness, our next goal was to minimize our energy loss from the method used to actuate the airfoil. Our criteria for determining our method of actuation were accuracy, power consumption, cost, and difficulty. Based on the design matrix above, the best option for us was a servo motor.

Due to our testing procedure requiring precise actuation and our limited access to specialized manufacturing equipment, our team chose electrical actuation as it is most precise and easy to use. For our prototype, we chose a Reefs RC 500 oz-in servo. The high-power servo was chosen to overcome the additional forces present in actuating a hydrofoil through water. In future design iterations, mechanical actuation may be investigated as an alternative to further minimize energy consumption.

Chapter 4: Calculations

4.1 Power Calculations

Calculating the predicted power our device should generate was important for three reasons. If COVID-19 shut down our plans to complete the build and finish testing, we wanted to have a mathematical representation of the power our device should theoretically produce. The second reason was for being able to compare our experimental results to the calculated predictions. The last reason was to determine if we had selected the correct generator. Overall, for a starting angle of attack of 78° , we determined the maximum power to be an average of 16.75 watts over a cycle of oscillation, according to our theoretical approximations.



Figures 13 & 14: Free body diagrams showing the forces of water on the hydrofoil and the resulting lift

To find power, we used Equation 29. The key contributing equations are those used to find the coefficient of lift, as seen in Equation 23, lift, as seen in Equation 25, and vertical velocity, as seen in Equation 28. The other equations include coefficient of lift, drag, and trigonometry used to determine vector components and the changing angle of attack.

Appendix A shows the full table of values for each contributing equation. Appendix B shows corresponding graphs to demonstrate trends of linear velocity, angular velocity, and power over time. From these graphs, the angular velocity, and thus the power, are cyclical. This comes from the conversion of linear motion to rotational motion through our slider-crank mechanism. When the shortest link is parallel to the longest link, the angular velocity reaches zero and relies on momentum to continue the cycle. At this instant, the generated power is zero. Conversely, when the shortest link is perpendicular to the longest link, the moment arm is at its longest, meaning the angular velocity, and thus, the power, are at their highest. This change in angular velocity reflects a changing actual radius. To account for this, the radius used to calculate the angular velocity at any given point in time will be equal to the horizontal component of the vector made by the smallest link. Thus, the maximum radius will be 6 inches while the minimum radius will act simply as a point.

Lift Coefficient:

$$C_L = \frac{2\pi\alpha}{1+\frac{2}{R}} \quad (23)$$

Drag Coefficient

$$C_D = \frac{C_L^2}{\pi R} \quad (24)$$

R is aspect ratio of the foil, α is angle of attack in radians

Lift:

$$L = C_L \rho v^2 A \quad (25)$$

Drag:

$$D = \frac{C_D \rho v^2 A}{2} \quad (26)$$

New angle of attack:

$$\alpha = \alpha_0 - \arctan\left(\frac{v_y}{v_x}\right) \quad (27)$$

Vertical Velocity:

$$\text{new vertical velocity} = \text{old vertical velocity} + \text{vertical acceleration} \times \text{change in time} \quad (28)$$

Power:

$$P = \tau * v_a \quad (29)$$

Where τ is torque and v_a is angular velocity.

4.2 Slider-Crank Mechanism

Our hydrofoil is estimated to move a total of 12 inches up and down. This makes our path length equal to 12 inches. To construct a slider-crank that has the output axis of rotation in line with the path of the slider, the link length of the crank must be half the path length. In turn the

length of the link turning the generator is 6 inches. To find the length of the second link we used the Grashof condition. The Grashof condition states that if the sum of the shortest and longest links is less than the sum of the other two links there can be a full 360-degree rotation of at least one of the links. Here our shortest link, S, is 0 inches because it is an in-line slider-crank linkage. Our longest link, L, is the ground link at 19.77 inches is derived from the distance between the point of rotation of the generator and the sliding mechanism. The other two links were chosen to be 6 inches and 14.4 inches, P and Q respectively.

$$S + L < P + Q$$

$$0 + 19.77 < 6 + 14.4$$

$$19.77 < 20.4$$

As you can see above the Grashof condition was satisfied with these link lengths. We also looked at the proportions of other in line crank-slider linkages to evaluate the proportions of our own. Since we had planned to attach our linkage outside of the frame of our device there was little consideration for interference in that regard. Once the lengths of the links were determined, we could then derive their instantaneous centers for use in determining the angular velocity.

In addition to design specifications in relation to dimensions of the frame and hydrofoil, we considered the linear and angular velocities of the links. To calculate these values, we used

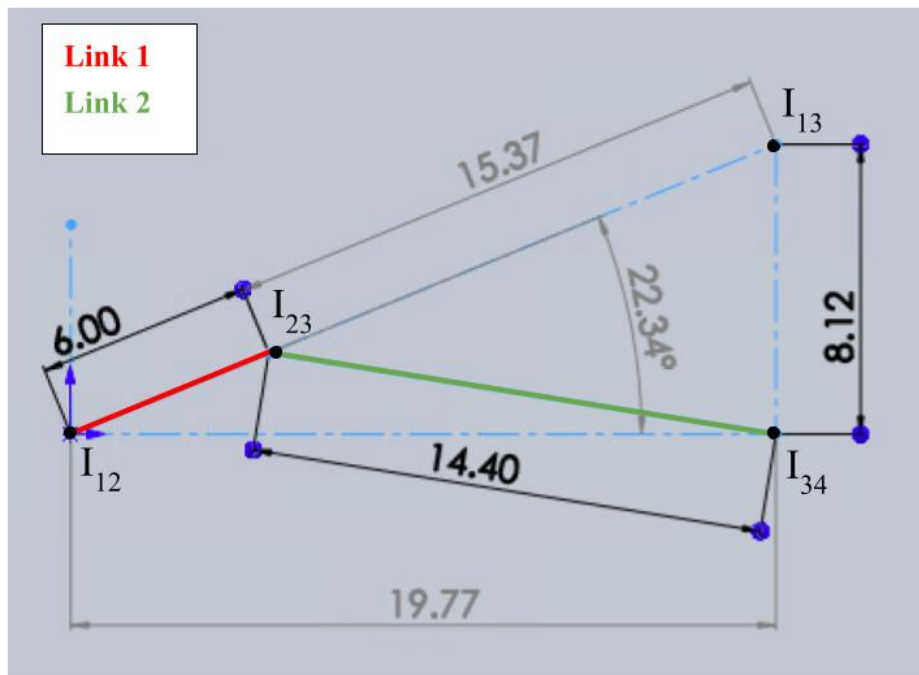


Figure 15: Solidworks design of slider-crank mechanism motion

the instantaneous center (IC) method. Using Solidworks we were able to find the position and distance between the ICs.

In the figure above you can see the two links in our slider-crank mechanism. Link 1, depicted in red, is the crank and attached to our generator. Link 2, depicted in green, attaches the crank to the linearly moving bearing. The four ICs that are used in our calculations are also shown. To find the angular velocity acting on our generator from the hydrofoil we used the following equations. $V_{hydrofoil}$ and the distances between the ICs are known, we were solving for ω_2 , V_{23} , and ω_1 .

$$V_{hydrofoil} = V_{34} \quad (30)$$

$$V_{34} = \omega_2 |I_{13}I_{34}| \quad (31)$$

$$V_{23} = \omega_2 |I_{13}I_{23}| \quad (32)$$

$$V_{23} = \omega_1 |I_{12}I_{23}| \quad (33)$$

$$\omega_1 = \frac{V_{23}}{|I_{12}I_{23}|} \quad (34)$$

Solving these equations systematically gave us ω_1 , the angular velocity, at a value of $9.93 \frac{rad}{s}$ acting on our generator, for the given linear velocity of the hydrofoil upon startup. Equation 31 was used to find the angular velocity of Link 2. The angular velocity of Link 2 is $3.81 \frac{rad}{s}$. Next Equation 32 was utilized to find the velocity of the joint between the links. The velocity of the joint between the links was $1.49 \frac{rad}{s}$. Finally, we used Equation 33 to find the angular velocity on Link 1, which is acting on our generator. As stated above, this was $9.93 \frac{rad}{s}$

$$\omega_2 = \frac{v}{8.12 \text{ in}} = \frac{0.80 \frac{m}{s}}{0.21 \text{ m}} = 3.81 \frac{rad}{s}$$

$$V_{23} = \omega_2 * 15.37 \text{ in} = 3.81 \frac{rad}{s} * 0.39 \text{ m} = 1.49 \frac{m}{s}$$

$$\omega_1 = \frac{V_{23}}{6 \text{ in}} = \frac{1.49 \frac{m}{s}}{0.15 \text{ m}} = 9.93 \frac{rad}{s}$$

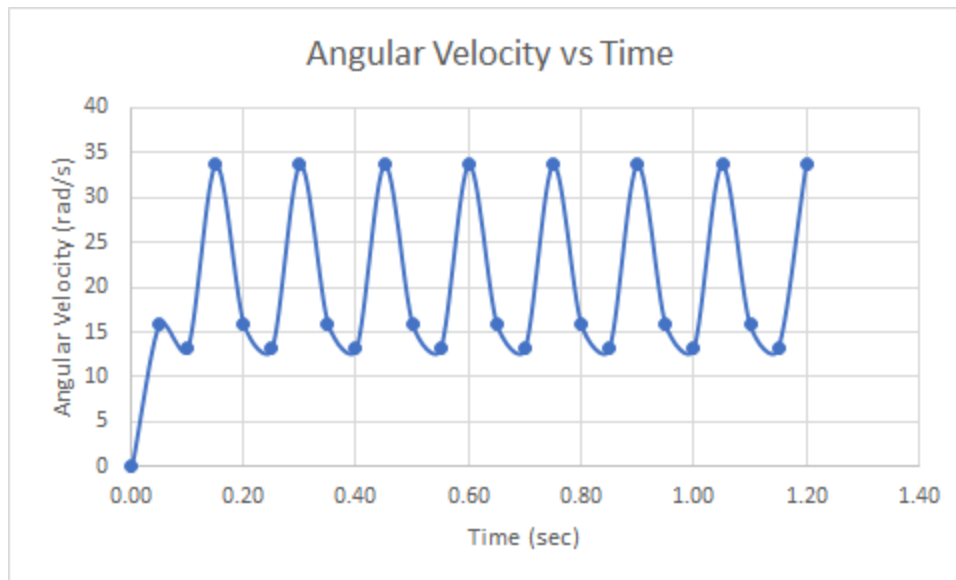


Figure 16: Angular velocity of the 6-inch rod about the generator

The graph above shows the cyclical nature of angular velocity, and thus power, over continuous oscillation of the foil. For this graph, we assumed torque would remain fairly constant.

Chapter 5: Construction

5.1 Foil

To fabricate our hydrofoil, our team created several wooden molds outlining our designed hydrofoil shape. The molds were used to hold an aluminum sheet, steel shaft, and wooden ribs in the desired shape. These wooden ribs were secured to the shaft and the sheet using multi-purpose Gorilla glue. Finally, to attain a neutrally buoyant weight, a combination of cement and expanding foam was added in between each rib until the density of the foil exactly matched that of water. To ensure our system was completely waterproof, we spray coated our hydrofoil with a rubber waterproofing solution.

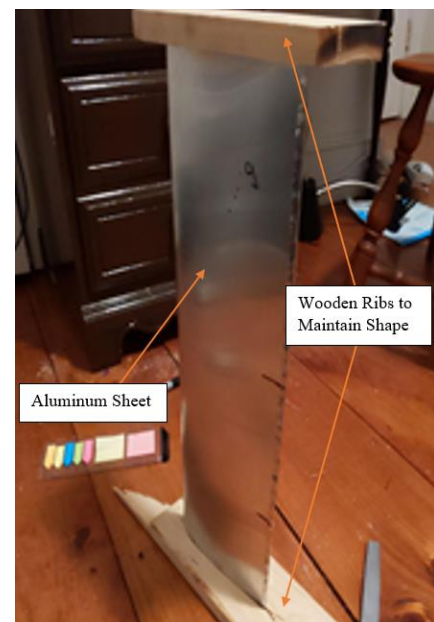


Figure 17: In-progress construction of hydrofoil using aluminum skeleton held in place by support ribs

5.2 Servo-Foil Attachment

To attach the foil to both the servo and the frame, we developed two adapters using Solidworks models and machined them from aluminum. One part was created to attach the servo to the bearing that moves vertically on the rod and hold it in place. We made a separate

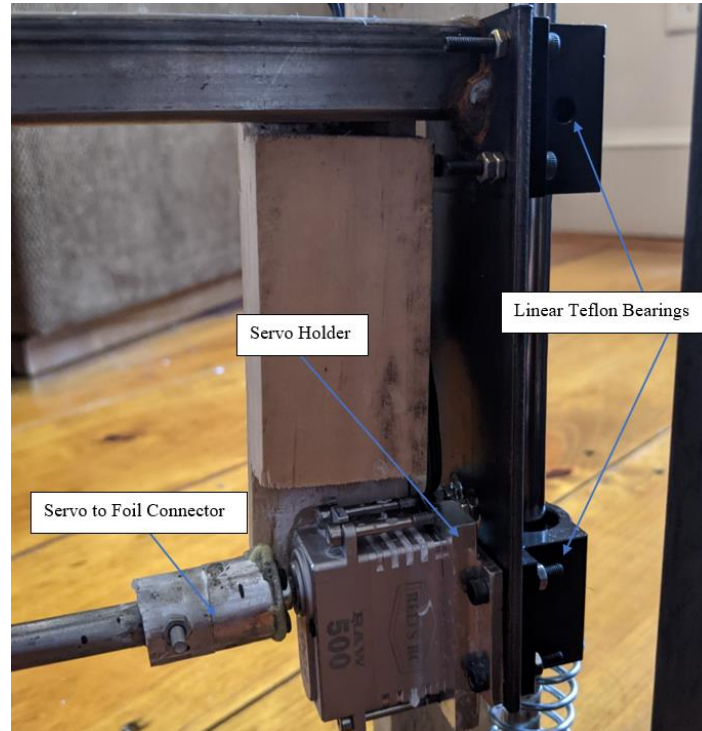


Figure 18: Assembled Servo- foil attachment and actuation system

component to attach the servo to the rod that runs through the foil, allowing the servo to rotate it. To attach the foil to the bearing on the other side of the frame, we created an adapter that attaches to the bearing and holds a smaller bearing that the foil's rod fits in, allowing it to rotate freely when actuated by the servo.

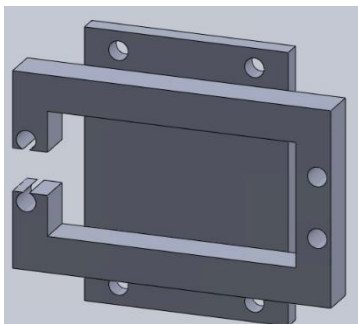


Figure 19: Solidworks design of servo holder seen fabricated in Figure 18

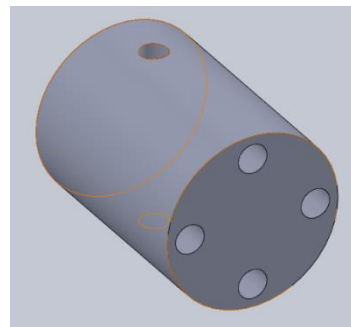


Figure 20: Solidworks model of servo-foil connector shown fabricated in Figure 18

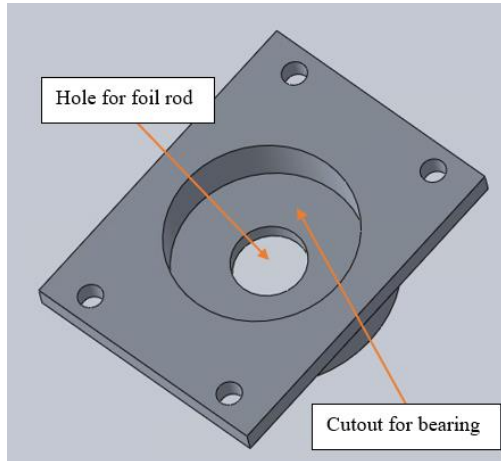


Figure 21: Solidworks model of bearing-foil adapter showing bearing seating position and foil rod position

5.3 Frame

In order to reduce chance of frame failure and to maximize rigidity, we chose to MIG weld all steel frame connections. However, if necessary, our frame design had the flexibility to be constructed using common power tools by drilling holes at the corners to be connected with nuts and bolts.



Figure 22: Example of MIG weld on steel frame

5.4 Slider-Crank Mechanism

The slider-crank mechanism was developed in Solidworks before being 3D printed with PLA plastic (See Figure 11). In order to fit on the print bed, the longest link was sectioned and a connecting application was devised as seen below. This allowed the full link to be printed while maintaining its mechanical ability to exert force within

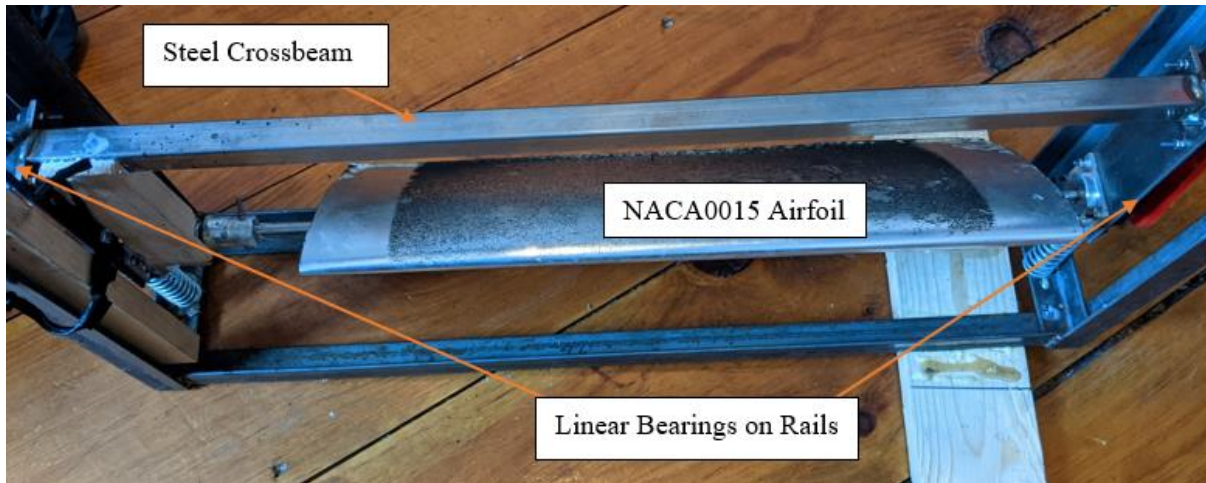


Figure 23: Assembled hydrofoil oscillation system showing fabricated foil, support crossbeam and bearing-rail assembly.

the linkage system. Additionally, the link connecting to the shaft of the generator has one hole that is smaller so there will be an interference fit between the link and the shaft.

5.5 Servo Actuation Method

To actuate the servo and change the angle of attack, we decided to use IR distance sensors to detect when the system had reached the peak of its oscillation accurately and consistently. We used an Arduino to code these sensors and allow them to communicate with our servo. We then used Rubber waterproofing spray on the entire electrical system that would be submerged to ensure watertight operation. Finally, these sensors were connected to the frame at the top and bottom of the oscillation amplitude as seen in Figure 25.

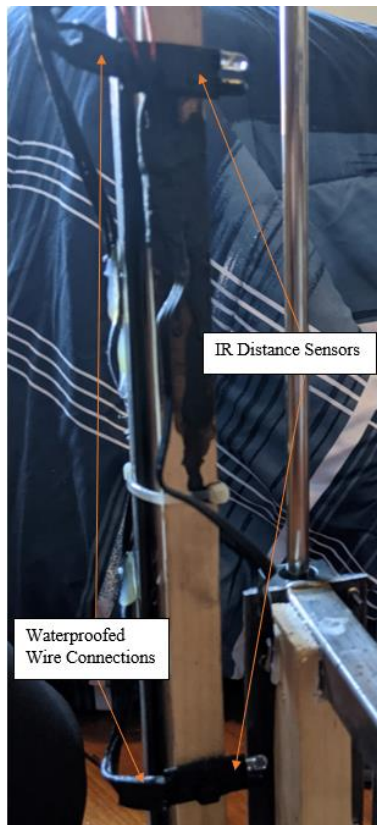


Figure 25: Fabricated Servo Actuation circuit with IR distance sensors

The servo motor and sensors were powered by a 7 cell 3300 mAh Nickel Metal Hydride (NiMH) battery pack as seen in Figure 26. All water sensitive electronics that did not need to be submerged were housed above the frame in a waterproof container shown in the final assembly (Figure 27).



Figure 24: Fabricated and assembled slider-crank mechanism showing slider rail, 4-bar linkage, and attachment points

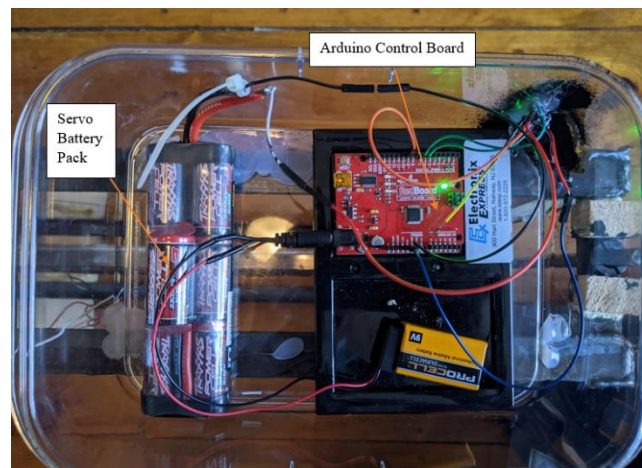


Figure 26: Waterproof electronics bay for powered systems

5.6 Assembly

Once the frame, foil, slider-crank mechanism, and connecting pieces were created, we assembled them into the final prototype. We used journal bearings to connect the foil to the rails of the frame. The servo motor attachment system was bolted onto the device holding the servo inside. The generator was connected to the frame with brackets, nuts, and bolts. The slider-crank mechanism was connected to the frame and the generator using nuts and bolts. The electrical system was wired up and soldered to the servo lead wires.



Figure 27: Completely assembled system with all subsystems attached

Chapter 6: Testing

6.1 Measurement Systems

To complete our testing, our team needed several measurement systems to record test data. The first, a velocimeter, was needed to determine the speed of the flowing water that our hydrofoil was oscillating in. For this, used a water-resistant velocimeter from WPI as we will not be submerging it for long periods of time and purchasing a fully waterproof design would be outside our budget. Secondly, we chose to use a digital multimeter to measure the power output. The multimeter will allow us to read the average voltage drop from the generator as the hydrofoil oscillates. This is a simple way to record the voltage drop of our system across a resistor which we could then use to derive power.

Overall, our system was designed and constructed to meet the design criteria laid out at the beginning of this section. The cost of all the material needed for our device came out to \$840 which is within our \$1000 budget. Additionally, where possible, our team opted for ease of manufacturability as the virtual and restricted nature of this academic year has made manufacturing very difficult. Finally, and most importantly, we have designed a system capable of harnessing energy from running water using an actuating hydrofoil and converting that energy into usable power using a linkage and a generator.

6.2 Testing Procedures

In the testing phase of this project, our team considered the following parameters as possible variables:

- Stream velocity
- Angle of attack
- Shape of airfoil
- Amplitude of oscillation
- Speed of actuation

Initially our team ruled out varying airfoil shape, stream velocity, and oscillation amplitude as they would all require additional machining and fabrication to control. Based on the remaining parameters, our team chose to focus on varying the angle of attack of our airfoil since this variable would give us a more significant and wide range of possible test values and results. Our

testing was intended to be conducted with the goal of using the angle of attack of our airfoil, both in pitching and heaving, to maximize our power output.

With our test variable determined, our team formulated a testing plan to hone our device on its optimal angle of attack. Our testing plan is outlined in the table below, utilizing the angle of attack values from Kinsey & Dumas (2008).

Angle of Attack	Duration of Test	Speed of Water	Power Generated
65	10 cycles at steady state	Recorded before each test	Recorded by a multimeter over 10 steady state cycles
68	10 cycles at steady state	Recorded before each test	Recorded by a multimeter over 10 steady state cycles
71	10 cycles at steady state	Recorded before each test	Recorded by a multimeter over 10 steady state cycles
74	10 cycles at steady state	Recorded before each test	Recorded by a multimeter over 10 steady state cycles
77	10 cycles at steady state	Recorded before each test	Recorded by a multimeter over 10 steady state cycles

Table 3: Testing plan to find optimal hydrofoil angle of attack

Each angle in the table above was intended to be tested three times, with the average of the power produced and the stream velocity taken. From this result, our team would have determined which range of angles contained the maximum power producing potential. From this, additional tests could be run between these two values to determine the optimal angle of attack.

COVID delayed our build progress, pushing initial testing back farther than originally anticipated. This time constraint meant we were only able to complete one set of tests. Upon arrival at our testing location, we measured the velocity at different parts of the stream. These velocities ranged from $0.5 \frac{m}{s}$ to $1.7 \frac{m}{s}$. As we began to set up our device for testing, we realized that it was not feasible due to the high force of the water requiring two people to hold the frame which would not leave enough hands to complete the test. Both the depth of the water and the force it applied on the foil contributed to this unsafe condition.

Rather than leave without results of any kind, we determined the next best course of action would be to test the foil on land. This would provide us with information on the efficacy of the mechanism used to translate the linear motion to rotational motion, and how much power this motion could produce. To do so, we set a timer running and manually oscillated the foil a set number of times, timing each oscillation. This simulated the foil being moved at different frequencies, as would be seen in a stream. While the foil was being oscillated by one person, a second person recorded the voltage output on a multimeter and a third person recorded the data.

With our adapted testing strategy, we devised a new data table, to record power, time, and frequency of oscillation. We set the duration and number of oscillations to make power our dependent variable. A sample of this table is shown in Table 4. The full version can be found in Appendix C.

Frequency: 1 Hz		
Duration [s]	Number of Oscillations	Power Produced [W]
10	10	
10	10	
10	10	
Average Power Produced:		

Table 4: Example of data collected in dryland testing

Three different frequencies, 0.67 Hz, 1.0 Hz, and 2.0 Hz, were tested three times each by using sets of different combinations of duration and number of oscillations. Table 4 above shows

one such set at a frequency of 1 Hz using a duration of 10 seconds at 10 oscillations. Once data was collected, the average power for that set could be determined.

Chapter 7: Results & Analysis

In testing, our team ran into several issues with our system which kept us from completing the original testing plan. Although we did have one positive result which was that our system oscillates at water velocities of 0.6-0.7m/s, it did so very slowly, producing negligible power. Additionally, in faster moving water we had several issues including: difficulty with the servo oscillating the foil quickly enough, the power draw from the servo quickly draining our battery, and difficulty with anchoring the testing device in fast moving water. Due to time constraints, we were unable to fix the issues necessary for a full water test to be completed. Instead, we tested our system mostly on dry land using forced oscillation and recorded the power output for different frequencies. This frequency range, which we chose to be between 0.67-2.0Hz, was determined based on the ranges we had found in our review of literature.

To test these frequencies on land, we manually oscillated the hydrofoil up and down while using a timer to maintain the desired frequency. This was accomplished by setting a timer for a certain number of seconds and manually lifting and lowering the foil a certain number of times in that period to achieve a desired frequency. At each test frequency, we measured voltage drop across a 2 kOhm Thevenin resistor (R_{th}) which was part of a Thevenin power circuit for maximum power output. This circuit consisted of a power source which was our generator and two equivalent 2 kOhm resistors in parallel. This circuit could be optimized for greater power output but due to our limited testing window we simply set the resistors equal to each other. We measured the voltage drop across one of the resistors. We repeated each frequency three times and took the average of the readings. Due to our severely shortened testing window, we were

unable to determine the optimized Thevenin resistance before testing and therefore resorted to a Thevenin resistance equal to the load resistance.

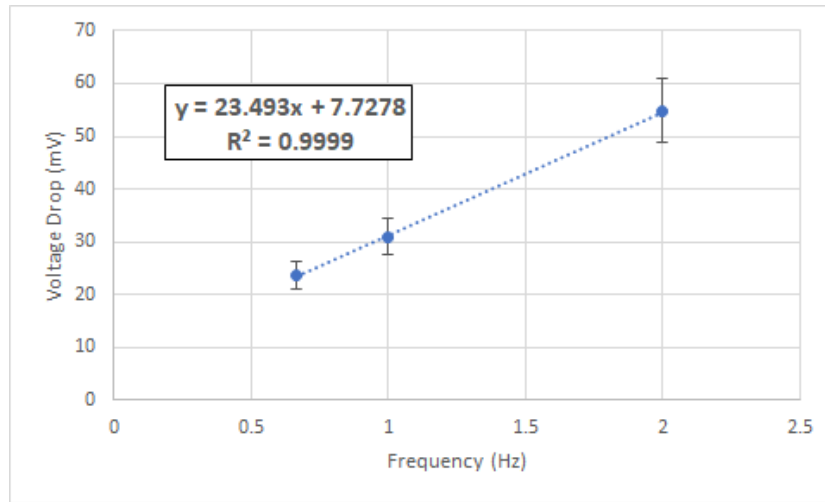


Figure 28: Graph showing frequency versus voltage drop across Thevenin resistor

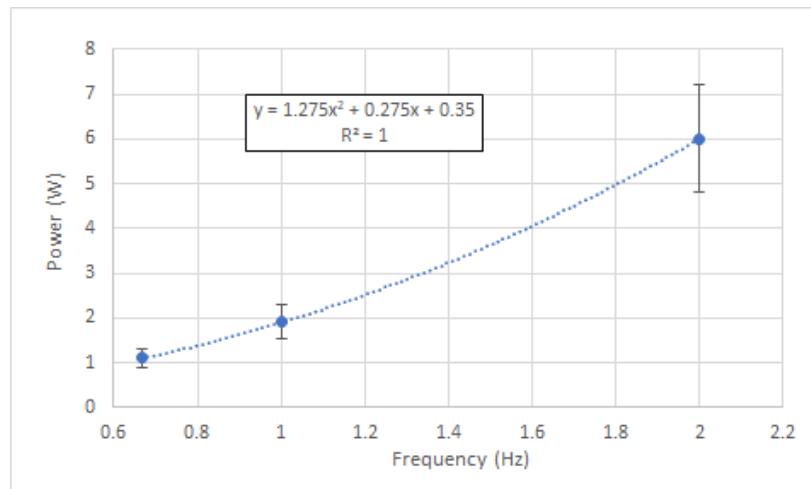


Figure 29: Power output versus frequency of hydrofoil oscillation

To analyze our results, we took the average of our voltages at each frequency and then used our equivalent resistance to derive power with the following equation:

$$P_{max} = \frac{V_{th}^2}{4 * R_{th}}$$

A graph comparing our calculated power output with oscillation is shown in Figure 29. We analyzed our data using an 2nd order polynomial fit which is what we expected since voltage increases linearly with oscillation and power increases as a second order polynomial with

voltage. Due to the nature of our testing, there is a significant amount of deviation which is most likely due to our oscillation amplitude not being exactly constant.

Even though our system was not able to be tested in water, we decided to compare our system at different, dryland, oscillation frequencies to the data we had found in the literature. These tests were not at all equivalent but by comparing the same frequencies, we were able to at least get an idea of how our system performed compared to similar systems. To determine the efficiency of our system and how it compared to the previous literature, we used our theoretical values for power and compared them to our estimates from testing. These theoretical values were based on the total power available the water running over the foil. Table 5 shows the comparison.

Frequency (Hz)	Max Theoretical Power (W)	Experimental Power (W)	Experimental Power /Max Power
0.67	19.3	1.1	5.6%
1	34.4	1.9	5.5%
2.0	77.4	6	7.7%

Table 5: Comparison of power ratios calculate at different testing frequencies

Due to the lack of water velocity, we decided to focus on the amount of power our system produced compared to the maximum power available instead of comparing efficiencies directly to literature. These results, seen in Table 5, do not account for the effects water may have on the system’s ability to convert linear motion to rotational motion. As such, this is more of a simulation assuming these effects are negligible. It is reasonable to look at expected power versus experimental power in this context, however, because the foil was oscillated at frequencies that would be seen in the water. Therefore, the power we recorded during dryland testing should emulate the power produced by the same frequencies of oscillation in a stream.

The power ratios we found were well below what we had expected. The two major factors that likely caused such low ratios were our choice of a 10W, low torque, high speed generator and our linkage being designed to rotate the generator only once per oscillation. This resulted in the generator applying virtually no load to the oscillation and thereby drawing much less power than expected. We theorize that the use of a much higher torque geared generator

would offer a significant improvement in the amount of power generated at each frequency, leading to higher power ratio.

We also were able to find some additional results as a byproduct of our testing. Firstly, with the velocity range of our in-water testing being 0.5-1.7m/s, we found that toward the upper end of stream velocity, it became increasingly difficult to secure our device in the stream, additionally, as the speed of the water increased, our servo's ability to oscillate the foil diminished significantly. These results are further discussed in our recommendations.

Chapter 8: Conclusions

The original aim of this project was to determine the optimal angle of tilt for our hydrofoil which would result in maximum efficiency in power generation. However, due to our very limited testing and inability to complete a full in-water test, we were not able to determine which angle led to maximum efficiency. Our focus then became determining which loading conditions from the generator worked best for our power generation. Given the limited time, we tested three different frequencies. However, to get a fuller picture of what the trends truly are, more frequencies should be tested.

We found that as we increased the oscillation of our system, power production increased as a 2nd order polynomial. However, this trend would lead to our system maximizing power at high oscillation which would be dangerous to aquatic wildlife which negates a main objective of our project. Therefore, we determined that employing a high torque, low rpm generator would allow us to maximize efficiency at low oscillation frequencies, maintain safe operation for aquatic life. We concluded that the optimal speed to operate at would be around 1 Hz since any slower than this may put the device in danger of stalling while any faster would needlessly endanger marine wildlife.

Chapter 9: Recommendations

Our device has much room for improvement. We believe that with more time or resources, changes can be made to the design that would significantly improve power generation. In addition, many of our components were designed and constructed based on what we had available to us and for short term use, but if this device were to be produced commercially,

components can be made better and with longer term use in mind. Overall, recommendations include:

- Connect the rod of the foil rigidly to the servo, or eliminate the need for a servo by mechanically altering the foil angle

If the connection between the foil and servo is unstable, the foil will not oscillate smoothly and may bind. While strengthening this connection would be an improvement, eliminating the need for a servo altogether would both increase stability and net power produced.

- Increase size and amperage output of power source to help servo actuation

In testing, our servo had a lot of difficulty turning the foil at higher water velocities. This could have been due to the low amperage output of our battery (3-amp max) or its low capacity (3300mAh). Increasing one or both of these parameters might improve our systems performance.

- Build the frame to allow for one alternator rail to be repositioned while the other remains rigid

When first constructed, the alternator rails were not precisely aligned, requiring additional time spent reconfiguring the frame. Enabling one rail to be adjusted will eliminate the need to make alterations to the frame after fabrication and compensate for human error in alignment.

- Develop an anchoring system for the device to use while testing

We were unable to test the foil in a stream due to the forces from the moving water. Our current design rests on top of the stream bed and was not heavy enough to remain in one place on its own. It was challenging to hold in place because the force on the foil was high. We determined that keeping both ourselves and the device upright while submerged in moving water was not feasible given our current design.

- Test a small-scale model of the current design for proof-of-concept

Along with an anchoring system, reducing the overall scale of the model will facilitate easier testing. With a smaller foil, the same speed of water will produce less force due to reduced area, thereby making it reasonable to stabilize the model in a safe way. A smaller foil can also be tested in shallower water, which is safer for those testing the device.

- Translate linear to rotational motion with a more effective method than a slider-crank mechanism

The way our slider-crank mechanism was designed only allows for one rotation of the generator with each oscillation of the foil. If the translation of motion enabled the generator to turn more than once per cycle of the foil, this would lead to greater power output.

Chapter 10: Global Impact

10.1 Engineering Ethics

We have used our knowledge of engineering principles and energy generation to enhance human welfare through the development and testing of our project. Through this process, we were impartial to our biases, designing for the greater good and not simply based on the design process we wanted to use. Through this work we have increased both the competence and prestige of the engineering field. We accomplished this by testing the familiar concept of a wind turbine to generate power in a new orientation and environment.

10.2 Societal and Global Impact

Our design can be realistic for implementation in National Parks once the design is fully developed and its efficacy is proven. The compact, unobtrusive design will provide green energy in sufficient supply without disrupting wildlife or views. Since the design is stand alone, it can be used in locations without connection to the grid. This means it has the potential for use beyond National Parks. The simplicity, small profile, and off-grid capabilities enables future expansion of use into remote regions across the country and around the world. While the size of the device itself will not increase, production and implementation would scale-up for widespread use. Such scale-up would involve a streamlined approach to production and further testing to ensure reliable efficacy of the device.

10.3 Environmental Impact

Coincident with the Engineering ethics laid out by ASME, our project aims to have minimal negative impact on the environment. It will contribute to reducing emissions by offering an alternative green source. When choosing the scale and design of our product, we noted the harm other green energy methods have on the environment, such as harming birds, fish, and

ocean floors. Contrastingly, our compact design allows fish to pass around and through with minimal disturbance. The small stream bed footprint will have limited impact on its location.

10.4 Codes and Standards

Since our product is still in the prototyping phase, specific codes and standards are something to consider further along in the development process. When understanding these codes and standards becomes relevant, it will be important to investigate federal and state regulations governing waterways. Additional safety standards involve the safety of the structure, from electrical codes to the safety of having a permanent structure in a stream.

10.5 Economic Impact

With a small-scale device such as our prototype, the cost to manufacture one will be fairly small. We were able to construct our prototype well within our \$1000 budget, and with larger scale manufacturing resources as well as a large amount of room for design improvements, it is reasonable to estimate production at a few hundred dollars per device, or even less. That would make this a competitive option in the market for small scale clean energy.

References

- Arof, H., Wijono, & Nor, K. M. (2005, June 6). Linear Generator: Design and Simulation. Retrieved October 15, 2020, from <https://ieeexplore.ieee.org/document/1437463/authors>
- Ballisty, T. (2015, May 21). Floodwater's Underrated Power. Retrieved October 11, 2020, from <https://weather.com/storms/severe/news/power-flood-water-20130704>
- Benson, T. Inclination Effects on Lift. (2018, April 5). Retrieved October 12, 2020, from <https://www.grc.nasa.gov/www/k-12/airplane/incline.html>
- Bent, G. C., & Waite, A. M. (2013). Equations for estimating bankfull channel geometry and discharge for streams in Massachusetts. *Scientific Investigations Report*. doi:10.3133/sir20135155
- Bernitsas, M., Ben-Simon, Y., Raghavan, K., & Garcia, E. (2009, February 01). The VIVACE Converter: Model Tests at High Damping and Reynolds Number Around 105. Retrieved October 14, 2020, from <https://asmedigitalcollection.asme.org/offshoremechanics/article/131/1/011102/456355/The-VIVACE-Converter-Model-Tests-at-High-Damping>
- Bernitsas, M., Raghavan, K., Ben-Simon, Y., & Garcia, E. (2008, November 01). VIVACE (Vortex Induced Vibration Aquatic Clean Energy): A New Concept in Generation of Clean and Renewable Energy From Fluid Flow. Retrieved October 11, 2020, from <https://asmedigitalcollection.asme.org/offshoremechanics/article/130/4/041101/471896/VIVACE-Vortex-Induced-Vibration-Aquatic-Clean>
- Bureau of Reclamation, L. (2018, August 1). HOOVER DAM. Retrieved October 11, 2020, from <https://www.usbr.gov/lc/hooverdam/faqs/powerfaq.html>
- Diltz, N., Gagnon, J., O'Connor, J., Wedell, J. (2017, April 20). Vortex Induced Vibration Energy Harvesting through Piezoelectric Transducers. Retrieved October 11, 2020 from https://web.wpi.edu/Pubs/E-project/Available/E-project-042117-160415/unrestricted/VIV_Final_Paper.pdf
- Dhar, M. (2017, December 06). How Do Solar Panels Work? Retrieved October 11, 2020, from <https://www.livescience.com/41995-how-do-solar-panels-work.html>
- The Editors of Encyclopaedia Britannica. (2016, October 25). Froude number. Retrieved October 11, 2020, from <https://www.britannica.com/science/Froude-number>
- Energy.gov. (n.d.). Microhydropower Systems. Retrieved October 11, 2020, from <https://www.energy.gov/energysaver/buying-and-making-electricity/microhydropower-systems>
- Energy Storage Association. (2020, September 24). Advanced Energy Storage Technologies. Retrieved October 15, 2020, from <https://energystorage.org/why-energy-storage/technologies/>
- Ericsson, L. (2012, October 03). Karman Vortex Shedding and the Effect of Body Motion. Retrieved October 14, 2020, from <https://arc.aiaa.org/doi/10.2514/3.50837>

- Farrell, J. (2018, March 29). Solar Surprise: Small-Scale Solar a Better Deal than Big. Retrieved October 11, 2020, from <https://www.renewableenergyworld.com/2018/03/29/solar-surprise-smallscale-solar-a-better-deal-than-big/>
- Festo. (n.d.). DualWingGenerator. Retrieved October 11, 2020, from <https://www.festo.com/group/en/cms/10222.htm>
- Geothermal Energy. (2017, May 9). Retrieved October 11, 2020, from <https://archive.epa.gov/climatechange/kids/solutions/technologies/geothermal.html>
- International Renewable Energy Agency. (n.d.). Geothermal. Retrieved October 11, 2020, from <https://www.irena.org/geothermal>
- Karow, M. (2019, December 2). Flag of the Future. Retrieved October 11, 2020, from <https://weatherology.com/trending/articles/Flag-Future.html>
- Kahan, A. (2019). U.S. Energy Information Administration - EIA - Independent Statistics and Analysis. Retrieved October 08, 2020, from <https://www.eia.gov/todayinenergy/detail.php?id=41433>
- Khan Academy. (2020). What is buoyant force? Retrieved October 11, 2020, from <https://www.khanacademy.org/science/physics/fluids/buoyant-force-and-archimedes-principle/a/buoyant-force-and-archimedes-principle-article>
- Kinsey, T., & Dumas, G. (2008). Parametric Study of an Oscillating Airfoil in a Power-Extraction Regime. *AIAA Journal*, 46(6), 1318-1330. doi:10.2514/1.26253
- Lee, J., & Bernitsas, M. (2011, September 09). High-damping, high-Reynolds VIV tests for energy harnessing using the VIVACE converter. Retrieved October 11, 2020, from <https://www.sciencedirect.com/science/article/pii/S002980181100134X>
- Liu, Z., Tian, F., Young, J., & Lai, J. (1970, January 01). Flapping foil power generator performance enhanced with a spring-connected tail. Retrieved October 11, 2020, from <https://aip.scitation.org/doi/full/10.1063/1.4998202>
- Lund, J. (2018, April 30). Environmental effects and economic costs. Retrieved October 11, 2020, from <https://www.britannica.com/science/geothermal-energy/Environmental-effects-and-economic-costs>
- Moore, A. (2019, November 13). Renewable Energy Poses Challenge For Wildlife Conservation. Retrieved October 11, 2020, from <https://cnr.ncsu.edu/news/2019/11/renewable-energy-poses-challenge-for-wildlife-conservation/>
- Nanomotion. (2018, August 28). The Piezoelectric Effect - Piezoelectric Motors & Motion Systems. Retrieved October 11, 2020, from <https://www.nanomotion.com/nanomotion-technology/piezoelectric-effect/>
- National Geographic Society. (2012, October 09). Hydroelectric Energy: The Power of Running Water. Retrieved October 11, 2020, from https://www.nationalgeographic.org/article/hydroelectric-energy-power-running-water/?utm_source=BiblioRCM_Row

- National Park Service. (2016, October 17). Onshore Wind Energy. Retrieved October 11, 2020, from <https://www.nps.gov/subjects/renewableenergy/onshorewind.htm>
- National Park Service. (2016, September 21). Offshore Wind Energy. Retrieved October 11, 2020, from <https://www.nps.gov/subjects/renewableenergy/offshorewind.htm>
- National Park Service. (2016, September 21). Solar Energy. Retrieved October 11, 2020, from <https://www.nps.gov/subjects/renewableenergy/solar.htm>
- National Park Service. (2020, March 10). Geothermal Energy. Retrieved October 11, 2020, from <https://www.nps.gov/subjects/renewableenergy/geothermal.htm>
- Office of Energy Efficiency and Renewable Energy. (n.d.). Advantages and Challenges of Wind Energy. Retrieved October 06, 2020, from <https://www.energy.gov/eere/wind/advantages-and-challenges-wind-energy> [A]
- Office of Energy Efficiency and Renewable Energy. (n.d.). How Do Wind Turbines Work? Retrieved October 06, 2020, from <https://www.energy.gov/eere/wind/how-do-wind-turbines-work> [B]
- Office of Energy Efficiency & Renewable Energy. (n.d.). Mesa Verde National Park. Retrieved October 11, 2020, from <https://www.energy.gov/eere/femp/mesa-verde-national-park> [C]
- Office of Energy Efficiency & Renewable Energy. (2017, April 18). 7 National Park Projects Enhanced by Clean Energy. Retrieved October 11, 2020, from <https://www.energy.gov/eere/articles/7-national-park-projects-enhanced-clean-energy>
- Office of Energy Efficiency & Renewable Energy. (n.d.). Renewable Energy: Utility-Scale Policies and Programs. Retrieved October 11, 2020, from <https://www.energy.gov/eere/slsc/renewable-energy-utility-scale-policies-and-programs> [D]
- Office of Energy Efficiency & Renewable Energy. (n.d.). Renewing Our National Parks. Retrieved October 11, 2020, from <https://www.energy.gov/eere/femp/renewing-our-national-parks> [E]
- Platzer, M., Ashraf, M., Young, J., & Lai, J. (2009). Development of a New Oscillating-Wing Wind and Hydropower Generator. *47th AIAA Aerospace Sciences Meeting including The New Horizons Forum and Aerospace Exposition*. doi:10.2514/6.2009-1211
- Piezo.com. (n.d.). Piezoelectric Energy Harvesters. Retrieved October 11, 2020, from https://piezo.com/collections/piezoelectric-energy-harvesters?_=pf
- Rosado, T. (1999). Hydrofoils. Retrieved October 11, 2020, from <https://web.mit.edu/2.972/www/reports/hydrofoil/hydrofoil.html>
- Runyon, J. (2018, March 29). Solar Surprise: Small-Scale Solar a Better Deal than Big. Retrieved October 11, 2020, from <https://www.renewableenergyworld.com/2018/03/29/solar-surprise-smallscale-solar-a-better-deal-than-big/>
- Sachs, G. (2016). Comparison of Power Requirements: Flapping vs. Fixed Wing Vehicles. *Aerospace*, 3(31), 1-15. doi:10.3897/bdj.4.e7720.figure2f

- Sullivan, R. (2014, March 11). Why do some birds flap their wings while others glide? Retrieved October 11, 2020, from <https://www.abc.net.au/science/articles/2014/03/11/3927566.htm>
- Sustainia. (2019, June 27). Smart Microgrids for Renewable Energy Access in Remote Areas. Retrieved October 11, 2020, from <https://goexplorer.org/smart-microgrids-for-renewable-energy-access-in-remote-areas/>
- Toothman, J., & Aldous, S. (2020, June 30). How Solar Cells Work. Retrieved October 12, 2020, from <https://science.howstuffworks.com/environmental/energy/solar-cell.htm>
- U.S. Energy Information Administration. (2020, March 24). History of Wind Power. Retrieved October 06, 2020, from <https://www.eia.gov/energyexplained/wind/history-of-wind-power.php>
- U.S. Energy Information Administration. (2019, November 5). How Electricity is Generated. Retrieved October 06, 2020, from <https://www.eia.gov/energyexplained/electricity/how-electricity-is-generated.php>
- Warren, C. (1953). A Theoretical Approach to the Design of Hydrofoils (pp. 1-22, Tech.). London, England: London: Her Majesty's Stationery Office.
doi:<http://naca.central.cranfield.ac.uk/reports/arc/rm/2836.pdf>
- Wilson, M. B. (1978). LIFTING LINE CALCULATIONS FOR HYDROFOIL PERFORMANCE AT ARBITRARY FROUDE NUMBER AND SUBMERGENCE (pp. 1-101, Tech.). Bethesda, Maryland: DAVID W. TAYLOR NAVAL SHIP RESEARCH AND DEVELOPMENT CENTER
- Yang, Z., Zhou, S., Zu, J., & Inman, D. (2018). High-Performance Piezoelectric Energy Harvesters and Their Applications. *Joule*, 2(4), 642-697. doi:10.1016/j.joule.2018.03.011
- Young, J., Lai, J., & Platzer, M. (2014, January 06). A review of progress and challenges in flapping foil power generation. Retrieved October 11, 2020, from <https://www.sciencedirect.com/science/article/pii/S0376042113000882>
- Young, J., Ashraf, M. A., Lai, J. C., & Platzer, M. F. (2013). Numerical simulation of fully passive flapping foil power generation. *AIAA journal*, 51(11), 2727-2739.
- Zhu, B., Zhang, W., & Huang, Y. (2019). Energy extraction properties of a flapping wing with a deformable airfoil. *IET Renewable Power Generation*, 13(11), 1823-1832. doi:10.1049/iet-rpg.2018.6193
- Zhu, Q., Haase, M., & Wu, C. H. (2009). Modeling the capacity of a novel flow-energy harvester. *Applied Mathematical Modelling*, 33(5), 2207-2217. doi:10.1016/j.apm.2008.05.027

Appendix A: Power Calculations

Distance	0	0.00	Angular Velocity	0.00	0.00	Lift Coefficient	5.13	Drag Coefficient	2.79	Lift [N]	1782.62	Velocity	1.28	Vertical Lift - Drag	1782.62	Vertical Acceleration	16.06	New Vertical Velocity Component	0.80	New water resultant vector Magnitude	1.28	New Alpha [rad]	0.68479935	Phi	0.6766	Phi in Deg	38.7638876
power [w]	0.00	0.00	Time [s]	0.00	0.00					970.71	Water Vel.	1872.62	1.28	996.23	16.06	8.98	1.25	1.25	1.28	0.68479935	2.29	0.46462468	0.8967	51.3789669			
0.062587	12.75	15.94	0.05	2.58	0.71	245.63	1474.89	1.28	229	1894.63	17.07	2.11	2.11	2.82	3.94	7.48	0.03909922	1.3223	75.7597796	8.26	0.02127453	1.3401	76.7810592				
0.167845	10.56	13.20	0.10	1.75	0.33	113.07	3176.99	2.29	3.50	1587.27	14.30	2.82	2.82	3.47	6.37	0.07112838	1.2902	73.9246443	8.77	0.0114737	1.3499	77.3426056					
0.308853	26.95	33.69	0.15	0.88	0.08	28.69	3759.71	3.50	5.03	1443.05	13.00	3.47	3.47	4.70	9.46	0.03909922	1.3223	75.7597796	8.26	0.02127453	1.3401	76.7810592					
0.482363	0.00	0.00	0.20	0.50	0.03	9.03	4343.38	5.03	6.37	3778.49	6.37	1043.72	9.40	3.94	7.48	0.03909922	1.3223	75.7597796	8.26	0.02127453	1.3401	76.7810592					
0.679379	0.00	0.00	0.25	0.27	0.01	2.65	3778.49	6.37	1043.72	9.40	3.94	7.48	0.03909922	1.3223	75.7597796	8.26	0.02127453	1.3401	76.7810592	8.77	0.0114737	1.3499	77.3426056				
0.892239	0.00	0.00	0.30	0.15	0.00	0.80	2862.79	7.48	7.48	2862.79	7.48	703.44	6.34	4.26	4.26	8.26	0.02127453	1.3401	76.7810592	8.77	0.0114737	1.3499	77.3426056				
1.114878	0.00	0.00	0.35	0.08	0.00	0.24	1899.89	8.26	8.26	1899.89	8.26	434.22	3.91	4.45	4.45	8.77	0.0114737	1.3499	76.7810592	8.77	0.0114737	1.3499	77.3426056				
1.343215	0.00	0.00	0.40	0.04	0.00	0.07	1154.81	8.77	8.77	1154.81	8.77	252.98	2.28	4.57	4.57	9.07	0.00613253	1.3552	77.648632	9.07	0.00613253	1.3552	77.648632				
1.574737	0.00	0.00	0.45	0.02	0.00	0.02	661.30	9.07	9.07	661.30	9.07	141.44	1.27	4.63	4.63	9.25	0.0032557	1.3581	77.8134622	9.25	0.0032557	1.3581	77.8134622				
1.807994	0.00	0.00	0.50	0.01	0.00	0.01	364.88	9.25	9.25	364.88	9.25	77.02	0.69	4.67	4.67	9.35	0.00172073	1.3596	77.9014094	9.35	0.00172073	1.3596	77.9014094				
2.042181	0.00	0.00	0.55	0.01	0.00	0.00	196.95	9.35	9.35	196.95	9.35	41.28	0.37	4.68	4.68	9.40	0.00090702	1.3604	77.9480317	9.40	0.00090702	1.3604	77.9480317				
2.276862	0.00	0.00	0.60	0.00	0.00	0.00	104.99	9.40	9.40	104.99	9.40	21.92	0.20	4.69	4.69	9.43	0.00047737	1.3609	77.9726486	9.43	0.00047737	1.3609	77.9726486				
2.511803	0.00	0.00	0.65	0.00	0.00	0.00	55.59	9.43	9.43	55.59	9.43	11.58	0.10	4.70	4.70	9.45	0.00025103	1.3611	77.9856168	9.45	0.00025103	1.3611	77.9856168				
2.746882	0.00	0.00	0.70	0.00	0.00	0.00	29.33	9.45	9.45	29.33	9.45	6.10	0.05	4.70	4.70	9.45	0.00013195	1.3612	77.9924397	9.45	0.00013195	1.3612	77.9924397				
2.982034	0.00	0.00	0.75	0.00	0.00	0.00	15.44	9.45	9.45	15.44	9.45	3.21	0.03	4.70	4.70	9.46	6.9341E-05	1.3613	77.996027	9.46	6.9341E-05	1.3613	77.996027				
3.217223	0.00	0.00	0.80	0.00	0.00	0.00	8.12	9.46	9.46	8.12	9.46	1.69	0.02	4.70	4.70	9.46	3.6435E-05	1.3613	77.9979125	9.46	3.6435E-05	1.3613	77.9979125				
3.452432	0.00	0.00	0.85	0.00	0.00	0.00	4.27	9.46	9.46	4.27	9.46	0.89	0.01	4.70	4.70	9.46	1.9143E-05	1.3613	77.9989032	9.46	1.9143E-05	1.3613	77.9989032				
3.687652	0.00	0.00	0.90	0.00	0.00	0.00	2.24	9.46	9.46	2.24	9.46	0.47	0.00	4.70	4.70	9.46	1.0057E-05	1.3613	77.9994238	9.46	1.0057E-05	1.3613	77.9994238				
3.922878	0.00	0.00	0.95	0.00	0.00	0.00	1.18	9.46	9.46	1.18	9.46	0.25	0.00	4.70	4.70	9.46	5.2839E-06	1.3614	77.9996973	9.46	5.2839E-06	1.3614	77.9996973				
4.158106	0.00	0.00	1.00	0.00	0.00	0.00	0.62	9.46	9.46	0.62	9.46	0.13	0.00	4.70	4.70	9.46	2.776E-06	1.3614	77.9998409	9.46	2.776E-06	1.3614	77.9998409				
4.393336	0.00	0.00	1.05	0.00	0.00	0.00	0.33	9.46	9.46	0.33	9.46	0.07	0.00	4.70	4.70	9.46	1.4584E-06	1.3614	77.9999164	9.46	1.4584E-06	1.3614	77.9999164				
4.628566	0.00	0.00	1.10	0.00	0.00	0.00	0.17	9.46	9.46	0.17	9.46	0.04	0.00	4.70	4.70	9.46	7.662E-07	1.3614	77.9999561	9.46	7.662E-07	1.3614	77.9999561				
4.863797	#REF!	#REF!	1.15	0.00	0.00	0.00	0.00	9.46	9.46	0.00	0.00	0.00	0.00	4.70	4.70	9.46	2.72271288	0	0	9.46	2.72271288	0	0	0			

Fixed Variables			
Aspect Ratio	3	Alpha [rad]	1.3613558
Water Density	997 kg/m ³	Mass	111 kg
Surface Area	0.696773 m ²	Delta T	0.05 s
Vertical Distar	0.3048 m	FoilLength	0.0762 m
Water Velocity	1 m/s		

Figure 30: Complete output of theoretical power calculations

Appendix B:

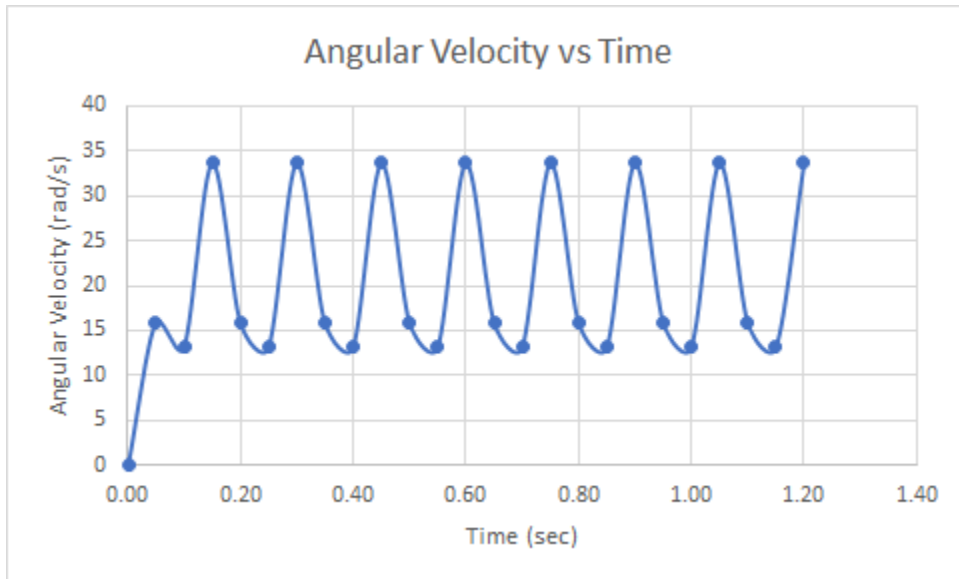


Figure 31: Graph of 6-inch linkage angular velocity as the foil oscillates

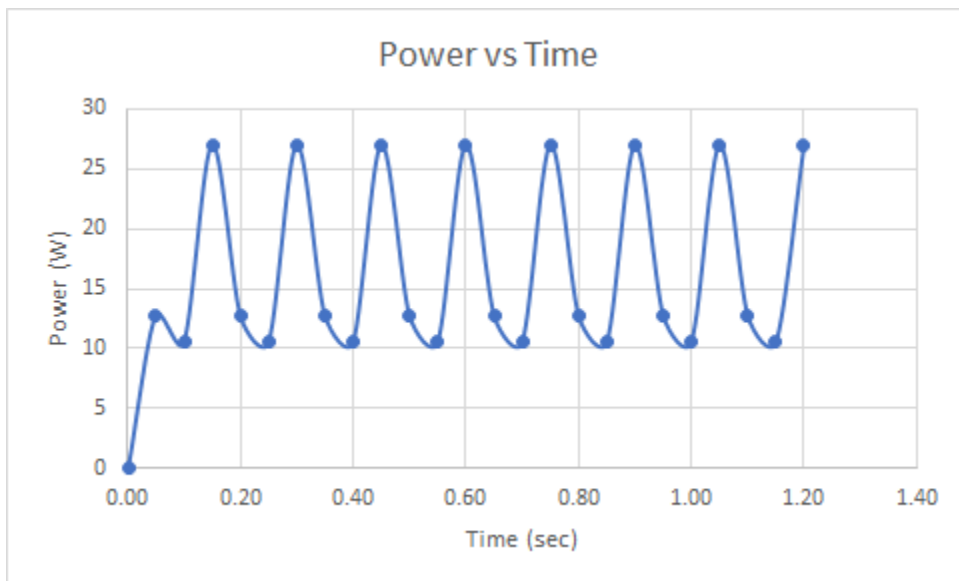


Figure 32: Instantaneous power produced by oscillation, varying with time

Appendix C: Sample Data Table

Frequency: 2.0 Hz		
Duration [s]	Number of Oscillations	Power Produced [mV]
5	10	
5	10	
5	10	
Average Power Produced:		
10	20	
10	20	
10	20	
Average Power Produced:		
15	30	
15	30	
15	30	
Average Power Produced:		
Overall Average Power Produced:		

Table 6: Sample data table for 2.0 Hz frequency testing

Appendix D: Data Collection

Frequency: 0.67 Hz		
Duration [s]	Number of Oscillations	Power Produced [mV]
12	8	21
12	8	21
12	8	23
Average Power Produced:		21.67
15	10	22
15	10	27
15	10	24
Average Power Produced:		24.33
30	20	23
30	20	25
30	20	26
Average Power Produced:		24.67
Overall Average Power Produced:		23.56

Table 7: All test values for 0.67 Hz frequency

Frequency: 1 Hz		
Duration [s]	Number of Oscillations	Power Produced [mV]
10	10	35
10	10	25
10	10	20
Average Power Produced:		26.67
15	15	34
15	15	37
15	15	35
Average Power Produced:		35.33
20	20	34
20	20	32
20	20	28
Average Power Produced:		31.33
Overall Average Power Produced:		31.11

Table 8: All test values for 1 Hz frequency

Frequency: 2 Hz		
Duration [s]	Number of Oscillations	Power Produced [mV]
5	10	49
5	10	58
5	10	52
Average Power Produced:		53
10	20	56
10	20	65
10	20	56
Average Power Produced:		59
15	30	47
15	30	55
15	30	51
Average Power Produced:		51
Overall Average Power Produced:		54.33

Table 9: All test values for 2 Hz frequency

Drawing of Crankshaft Link

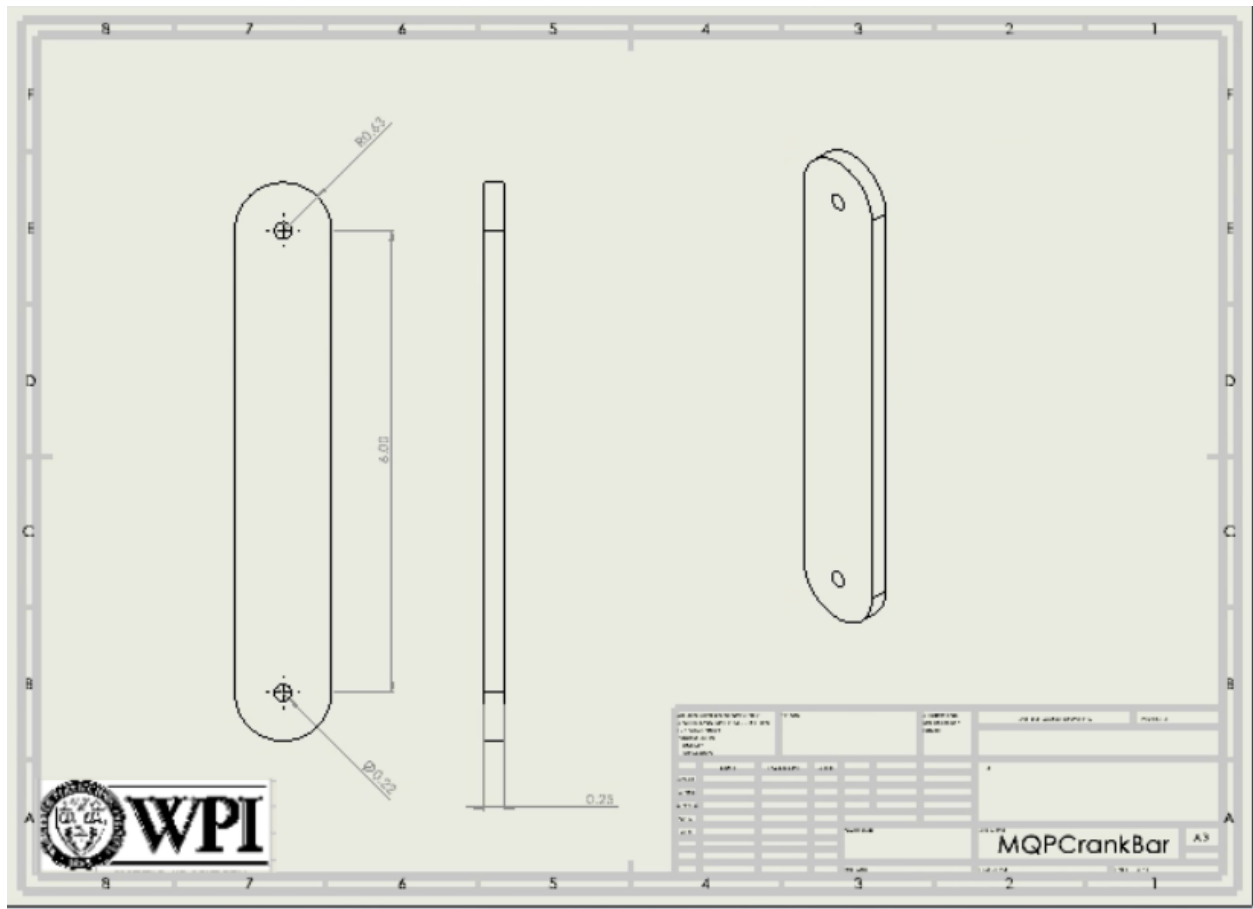


Figure 35: Design drawing for full crank shaft linkage

Drawing of the Connecting Link

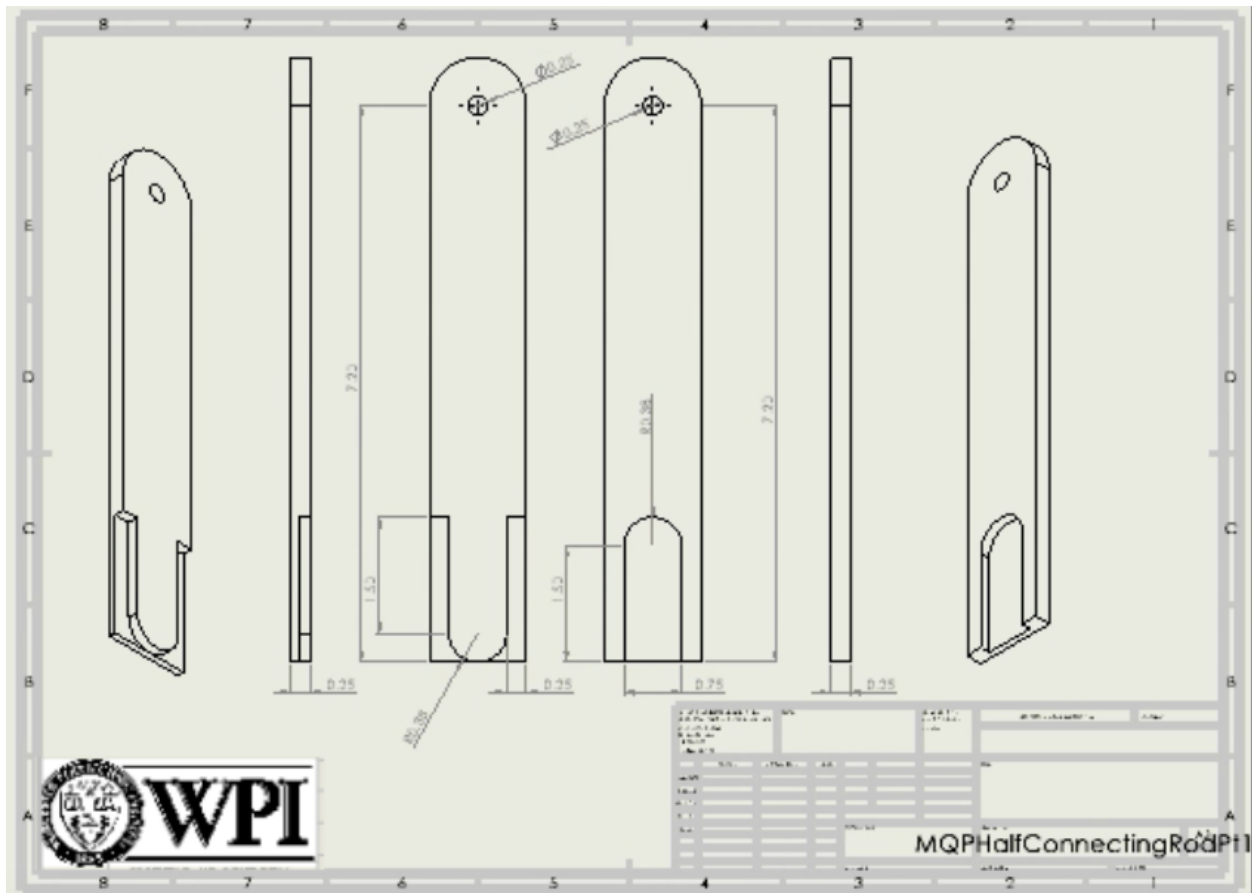


Figure 36: Design drawing for long 4-bar linkage